Multiradionuclide evidence for an extreme solar proton event around 2610 BP

Paschal O'Hare

Dissertations in Geology at Lund University,
Master's thesis, no 499
(45 hp/ECTS credits)

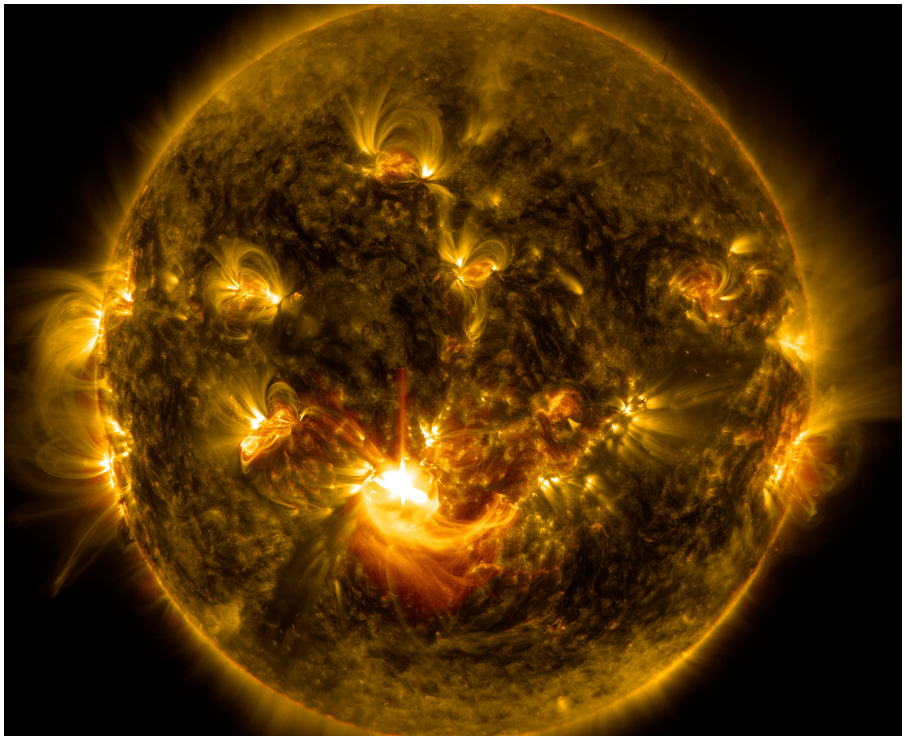

Department of Geology
Lund University
2017

Multiradionuclide evidence for an extreme solar proton event around 2610 BP

Master's thesis
Paschal O'Hare

Department of Geology
Lund University
2017

Contents

Cover Picture: NASA's Solar Dynamics Observatory captured this image of a mid-level solar flare – as seen in the bright flash in the middle –on Dec. 16, 2014 shortly before midnight EST.

Credits: NASA/SDO

Downloaded 03/07/2017 from: https://www.nasa.gov/sites/default/files/20141217-m8.7flare_171-131.jpeg

Abbreviations

AMS	Accelerator mass spectrometry
BP	Years before AD 1950
CGRN	Cosmogenic Radionuclide
F_{30}	Fluence (particles per cm2) above 30 MeV
GCR	Galactic cosmic-rays
GICC05	Greenland Ice Core Chronology 2005
GLE	Ground level event
GRB	Gamma-ray burst
GRIP	Greenland Ice core Project
GeV	Giga-electron volt
IntCal13	Northern Hemisphere atmospheric radiocarbon calibration curve
MeV	Million electron volt
NGRIP	North Greenland ice core Project
SCR	Solar cosmic-rays
$\Delta^{14}C$	^{14}C concentration corrected for fractionation and decay, relative to a standard

Multiradionuclide evidence for an extreme solar proton event around 2610 BP

PASCHAL O'HARE

O'Hare, M P., 2017: Multiradionuclide evidence for an extreme solar proton event around 2610 BP. *Dissertations in Geology at Lund University*, No. 499, 26 pp. 45 hp (45 ECTS credits)

Abstract: Recently it has been confirmed that extreme solar proton events (SPE) can lead to significantly increased production of cosmogenic radionuclides (Mekhaldi et al. 2015). The evidence of these events can be recorded in tree rings (^{14}C) and ice cores (^{10}Be, ^{36}Cl). The IntCal13 calibration curve, which is a continuous tree ring record of ^{14}C fluctuations throughout the Holocene, was used to locate two potential spikes in radionuclide production (~7510 and ~2610 BP). The primary aim of this study was to establish whether these potential spikes have counterparts in other radionuclide records. The secondary aim was to determine whether the spikes in radionuclide production could be attributed to extreme solar events, and to define the parameters of these events.

The results indicate an increase in ^{10}Be concentration and flux from the NGRIP ice core for the younger period of interest, 2610 BP. Additionally, a peak in concentration and flux has been discovered in existing GRIP ^{36}Cl records for the same period. This synchronous peak in both records is consistent with the increased radionuclide production expected due to an extreme SPE. Calculations based on the production yields of ^{10}Be and ^{36}Cl suggest that the hypothesised SPE around 2610 BP was characterised by a hard spectrum and a exceptionally high fluence. Furthermore, this event was at least an order of magnitude more energetic than the so far assumed strongest hard SPE of February 1956, and similar in magnitude to the remarkably strong hard AD775 paleo-SPE event.

Keywords: cosmic-rays, cosmogenic radionuclides, NGRIP, GRIP, solar proton event, SPE

Supervisor: Raimund Muscheler

Co-supervisor: Florian Mekhaldi

Paschal O'Hare, Department of Geology, Lund University, Sölvegatan 12, SE-223 62 Lund, Sweden. E-mail: paschal.ohare@gmail.com

Multiradionuclide bevis för en extrem sol proton event runt 2610 BP

PASCHAL O'HARE

O'Hare, M P., 2017: Multiradionuclide bevis för en extrem sol proton event runt 2610 BP. *Examensarbeten i geologi vid Lunds universitet*, Nr. 499, 26 sid. 45 hp.

Sammanfattning: Det har nyligen bekräftats att extrema solar proton events (SPE) kan leda till kraftigt ökad produktion av kosmogena radionuklider (Mekhaldi et al. 2015). Bevis för detta kan påträffas i trädringar (^{14}C) och iskärnor (^{10}Be, ^{36}Cl). Kalibreringskurvan IntCal13, vilken är ett kontinuerligt trädringsregister över ^{14}C fluktuationer under hela Holocen, användes för att lokalisera två potentiella toppar i radionuklidproduktion (ca 7510 och ca 2610 BP). Det främsta syftet med denna studie var att fastställa huruvida dessa potentiella toppar har motsvarigheter i andra radionuklida arkiv. Vidare var syftet att fastställa huruvida topparna i radionuklid produktion kan hänföras till extrema solar proton events, samt definiera parametrarna för dessa event.

Resultaten indikerar en ökning av ^{10}Be-koncentration och flöde från NGRIP-iskärnan för den yngre av de studerade perioderna, 2610 BP. Dessutom har en topp i koncentration och flöde upptäckts i befintliga GRIP ^{36}Cl arkiv för samma period. Denna synkrona topp i båda geologiska arkiv är överensstämmande med den ökade radionuklidproduktion som kan förväntas efter en extrem SPE. Beräkningar baserade på mängden producerad ^{10}Be och ^{36}Cl tyder på att den hypotiserade SPEn runt 2610 BP präglades av ett hårt spektrum och en exceptionellt hög fluens. Dessutom var detta event åtminstone en storleksordning starkare än det hittills förmodat starkaste hårda SPE i februari 1956 och i samma storleksordning som det anmärkningsvärt starka hårda AD775 paleo-SPE eventet.

Nyckelord: kosmiska strålar, kosmogena radionuklider, NGRIP, GRIP, sol proton händelse

Handledare: Raimund Muscheler

Co-Handledare: Florian Mekhaldi

Paschal O'Hare, Geologiska institutionen, Lunds Universitet, Sölvegatan 12, 223 62 Lund, Sverige. E-post: paschal.ohare@gmail.com

1 Introduction

This study was motivated by the identification of two distinct rapid changes in $\Delta^{14}C$ within the IntCal13 dataset, around 7510 and 2610 BP (henceforth LU7510 and LU2610; fig. 1).

The production of cosmogenic radionuclides such as ^{10}Be, ^{36}Cl and ^{14}C result from the nuclear cascade triggered when cosmic-rays enter the atmosphere and interact with nitrogen, oxygen and argon. The number of cosmic-rays which reach the Earth's atmosphere is primarily modulated by the intensity of the magnetic field generated by our Sun (the heliomagnetic field), and the Earth's geomagnetic field. The strength of this modulation changes on annual to millennial time scales (Vasiliev & Dergachev 2002), meaning that the concentration of cosmogenic radionuclides in archives such as tree rings and ice cores changes through time. However, the rapid changes in $\Delta^{14}C$ for LU7510 and LU2610 in IntCal13 suggest sharp increases in radionuclide production which are possibly unrelated to normal solar modulation.

Recently it has been confirmed that enormous solar storms can produce significant amounts of cosmogenic radionuclides which leave their imprint in tree rings (^{14}C) and ice cores (^{10}Be, ^{36}Cl) (Mekhaldi et al. 2015). It is hypothesised that such events may be responsible for the previously mentioned rapid $\Delta^{14}C$ changes in IntCal13. In the context of modern society, enormous solar storms pose a threat to communication, electronic and power systems (Schrijver et al. 2012). Therefore, better understanding the relationship between magnitude and occurrence frequency of such events is of great importance for solar physics, and safeguarding space technologies and modern technological infrastructure.

Cosmogenic ^{10}Be, ^{14}C and ^{36}Cl are produced in the atmosphere through a series of reaction pathways. The individual production rates for these radionuclides are differently sensitive to the kinetic energies of incident particles. This differing energy sensitivity can, in theory, be used to determine the energy spectrum and therefore the source of sharp peaks in cosmogenic radionuclide production.

In this study, new and sub-annually to annually-resolved ^{10}Be was measured from the North Greenland Ice Core Project (NGRIP) ice core and compared with other available cosmogenic radionuclides records in order to test for the presence, and assess the potential causes of the LU7510 and LU2610 events.

2 Background

2.1 Cosmic rays and the production of cosmogenic radionuclides

The Earth is constantly being bombarded by high energy particles in the form of cosmic radiation from interstellar space. These particles, which have been accelerated close to the speed of light, are commonly referred to as cosmic rays (Reasoner et al. 1968). α-particles and protons (helium and hydrogen nuclei stripped of their orbital electrons) form the majority of cosmic rays (~12% and ~87% respectively; Beer et al. (2012)). The cosmic radiation which reaches the Earth's atmosphere is limited by shielding in the form of both the geomagnetic field, produced by the Earth, and the heliosphere generated by our Sun. Variation in this shielding modulates the total flux of incoming energetic particles. Thus, periods of low solar activity lead to an increased amount of galactic cosmic rays reaching the Earth's atmosphere and vice versa (fig. 2).

The energy spectrum of incoming cosmic radiation, usually expressed in giga-electron volts (GeV), is relatively wide and can provide some insight

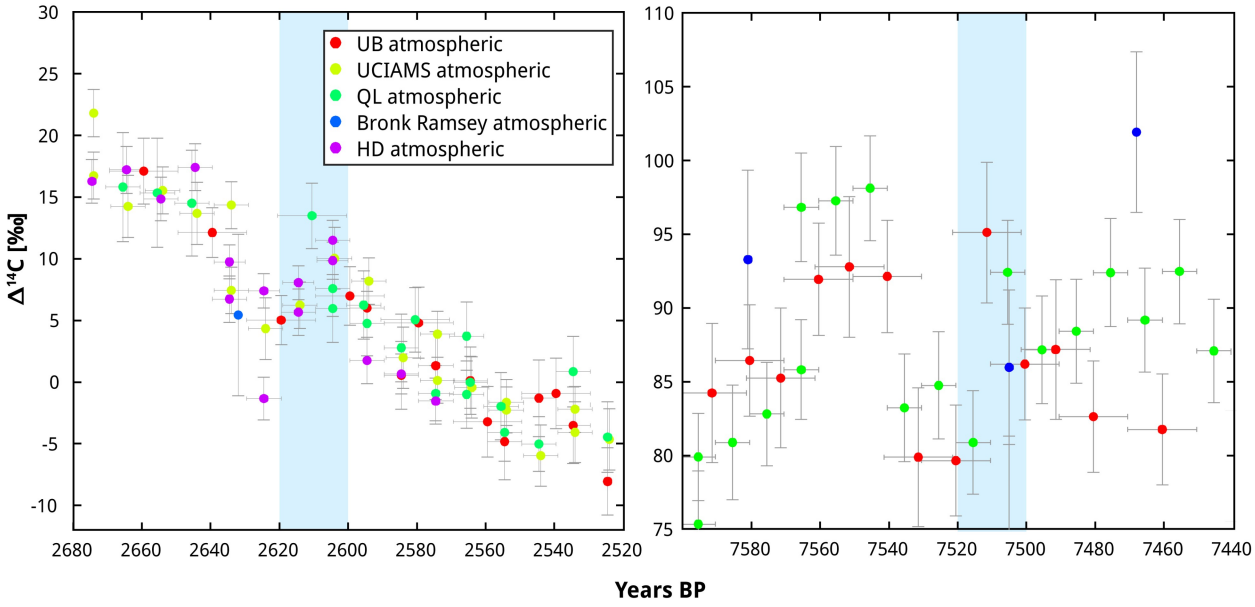

Fig. 1. IntCal13 $\Delta^{14}C$ measurements for the two suggested periods of interest (LU2610 and LU7510) where the raw data (grouped by dataset) in the ^{14}C calibration curve (Reimer et al. 2013) suggest the possibility of rapid ^{14}C increases. Vertical bars represent measurement error values, horizontal bars represent the time span that an individual measurement covers.

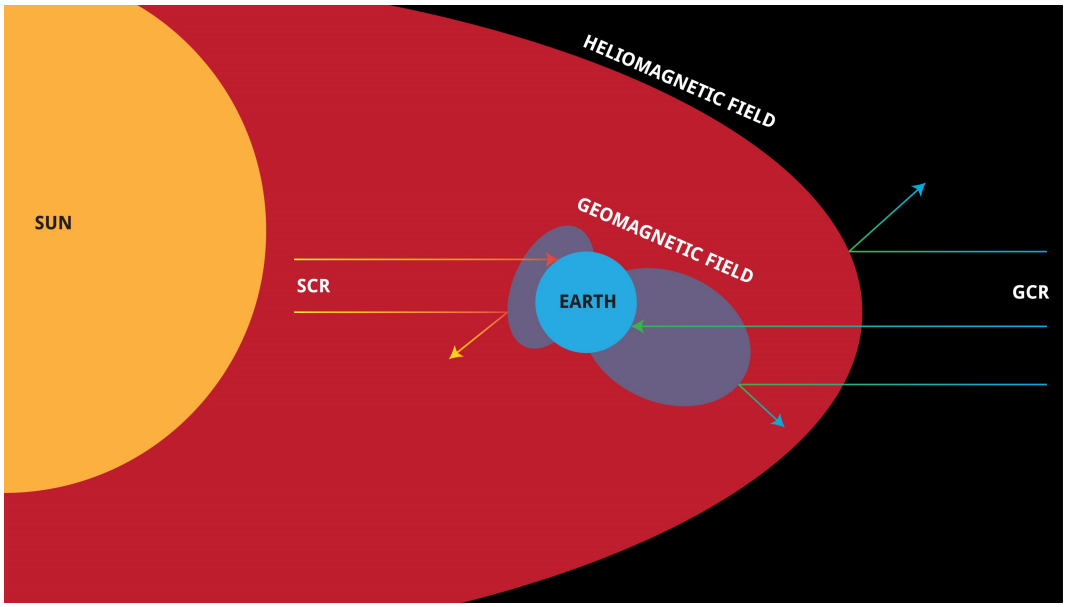

Fig. 2. Solar and geomagnetic modulation of Solar and Galactic cosmic rays (SCR and GCR respectively). Blue shading around Earth represents the geomagnetic field generated by Earth. Red shading represents the Sun's heliosphere. Deflection and penetration of both types of rays also indicated (adapted from Beer et al. (2012)).

into its sources. Particles less than 1 GeV are thought to have a solar origin, and are hence termed solar cosmic rays (SCR). Particles with energies higher than 1 GeV represent the "harder" end of the cosmic ray spectrum and originate from beyond the heliosphere, and are therefore termed galactic cosmic rays (GCR). GCR particles are hypothesized to originate from shock-wave-bound material ejected during the collapse and subsequent explosions of massive stars, also called supernova explosions (Koyama et al. 1995; Ackermann et al. 2013), the frequency of which (at a galactic level) produces a uniform level of GCR in our local interstellar system (Beer et al. 2012).

The interaction of cosmic radiation with the Earth's atmosphere leads to the production of cosmogenic radionuclides such as ^{14}C, ^{10}Be and ^{36}Cl. Therefore, rapid changes in production rates of these radionuclides indicate changes in the levels of cosmic radiation. The motivation of this study lies in the rapid increase in radiocarbon within two periods of the IntCal13 dataset, occurring around 2610 yr BP and 7510 yr BP. It is possible that these events may be explained by changes in solar modulation, so this will be the first line of enquiry. If solar modulation cannot explain the production rate increases of these events, other sources will be investigated, such as solar proton events (SPE), short gamma ray bursts (GRB) or relatively nearby supernovae explosions which result in longer gamma-ray bursts.

2.2 Production of cosmogenic ^{14}C, ^{10}Be, and ^{36}Cl

Primary cosmic rays which encounter the Earth's atmosphere trigger a nuclear cascade which results in the production of secondary particles (Masarik & Beer 1999). The resulting secondary particles, which include protons and neutrons, can then initiate spallation reactions involving the principal components of the atmosphere: nitrogen (N), oxygen (O) and argon (Ar). The formation of cosmogenic radionuclides is the result of these spallation reactions (Beer et al. (2012); Huggle et al. (1996); Yim & Caron (2006)). The main reaction pathways are shown in figure 3.

The abundance of individual nuclides produced during these spallation reactions is dependent on a combination of the energy required (incident energy from cosmic ray) to produce the reaction, as well as atmospheric abundance of target elements. Of the three nuclides considered here, ^{14}C is most abundantly produced due to having the smallest required incident energy and the highest abundance of the required base element ^{14}N. The production of ^{10}Be, arising from the the fission of ^{16}O and ^{14}N, requires a higher incident energy, resulting in a lower abundance. Finally, among the radionuclides mentioned so far, ^{36}Cl is the rarest as it forms primarily during the spallation of ^{40}Ar, which accounts for ~1% of atmospheric composition (Huggle et al. 1996).

Due to spatial variation in Earth's geomagnetic field and atmospheric structure, the production of cosmogenic radionuclides is latitude and altitude dependent. Lower cut-off rigidities and geomagnetic shielding at higher latitudes may result in larger cosmogenic radionuclide production relative to lower and mid latitudes (Shea & Smart 1970; Herbst et al. 2013). In addition, there is a production differential in terms of altitude, with most radionuclide production occurring in the lower stratosphere and upper troposphere (Beer et al. 2012).

The energy of incident cosmic rays has been shown to impact the production rate (relative to incoming particle energy) of individual cosmogenic radionuclides (Webber et al. 2007). Lower energy particles, usually sourced via SCRs, result in a different cosmogenic radioniuclide production 'signature' compared to higher energy particles (i.e.

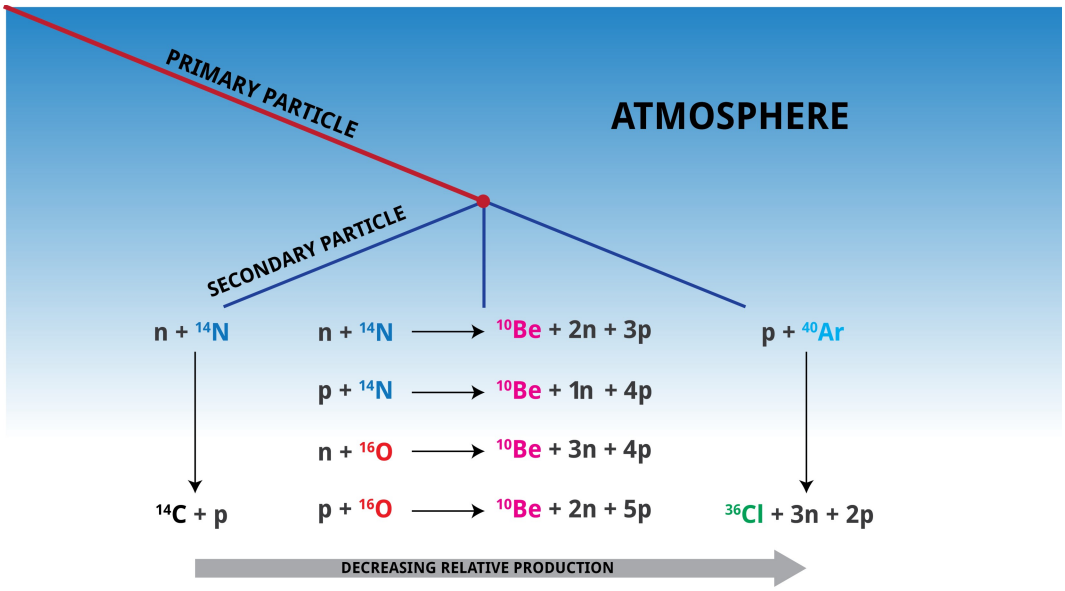

Fig. 3. Relative production of radionuclides in the atmosphere. Primary particles react into secondary particles which through spallation of ^{14}N, ^{16}O and ^{40}Ar produce resulting radionuclides. Main reaction pathways shown with increasing relative production from left to right. Adapted from Huggle et al. (1996); Yim& Caron (2006); Beer et al. (2012); Mekhaldi et al. (2015). Decreasing relative production is not the case for lower energy particles – where relatively more ^{36}Cl is produced at low energies.

GCR source). An example of such a change in signature occurs between the energy spectrum 0.01 to 0.1 GeV (specifically ~25-30MeV; see fig. 4), where there is a visible 'levelling out' in ^{36}Cl production, while $^{10}Be/^{14}C$ are decreasing with decreasing kinetic energy of incident particles. This trend highlights the sensitivity of ^{36}Cl production to lower energy (SCR) particles. Although GCR induced production accounts for much of the cosmogenic radionuclides of interest in this study, particularly large solar storms resulting in rapid increases in SCR could significantly increase the production of ^{36}Cl relative to ^{10}Be and ^{14}C.

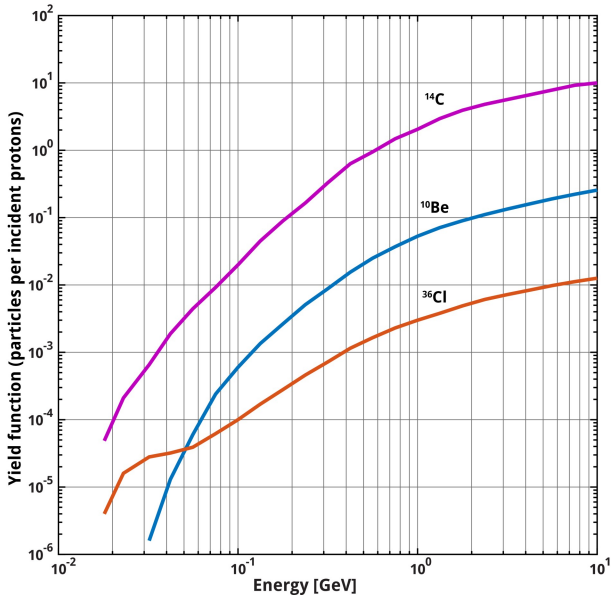

Fig. 4. Yield functions of various cosmogenic isotopes: ^{14}C (Castagnoli & Lal 1980), ^{36}Cl and ^{10}Be (Webber et al. 2007) in the atmosphere per incident vertical cosmic ray proton as a function of energy – modified from Mekhaldi et al. (2015).

In summary, cosmic ray-induced spallation reactions within the Earth's atmosphere lead to a series of complex nuclear cascades, resulting in the production of cosmogenic radionuclides. Each radionuclide entails different production pathways and target nuclei, and therefore is differently sensitive to the energy of incoming cosmic rays. The relative production of ^{36}Cl and ^{14}C (to a lesser extent) are generally more sensitive than ^{10}Be to lower-energy solar particles. These patterns of relative production yield differences can, in theory, be used to infer the energy level of incident cosmic rays for a given period (Mekhaldi et al. 2015).

2.3 Transport and deposition of cosmogenic ^{14}C, ^{10}Be and ^{36}Cl

^{14}C, ^{10}Be and ^{36}Cl records are widely used in the reconstruction of past solar activity. As seen in the previous section, their production rates vary widely in terms of production processes and incident particle energy spectra. In addition, the processes and mechanisms of transport and deposition for each radionuclide add further distinctions on how their relative abundances are interpreted in geological archives. The following section will outline the transport and deposition mechanisms for each.

2.3.1 Carbon-14

Carbon-14, which is produced through the neutron capture of nitrogen-14, is the most abundant of the three cosmogenic radionuclides discussed so far. It has a half-life of approximately 5.73 ka and, due to its involvement in the global carbon cycle, has the longest atmospheric residence time relative to the

aforementioned radionuclides (7-8 years; Beer et al. (2012)). After formation, ^{14}C can follow several pathways into various Earth system reservoirs. Primarily, it forms gaseous $^{14}CO_2$ and is absorbed into vegetation through photosynthesis or dissolved into the surface of the oceans. During the breakdown of organic matter, some of the absorbed ^{14}C is released back into the atmosphere or sequestered into soil. Over longer time scales, the ^{14}C dissolved into oceans is absorbed by calcareous organisms and sequestered to deeper ocean waters in the form of $Ca^{14}CO_3$, while also moving into the deep ocean via diffusion and ocean mixing. Some of this sequestered ^{14}C eventually returns to the atmosphere through upwelling of ocean waters and exchange with atmosphere. Therefore, the atmospheric concentration of ^{14}C, $N_a(t)$ is a function of the production rate $Q(t)$, the rate of decay $e^{-\lambda t}$ and the carbon cycle $C(\tau)$. The following equation (Beer et al. 2012) expresses this function as:

$$N_a(t) = \int_o^t Q(t) e^{-\lambda(t-\tau)} C(\tau) d\tau \qquad (1)$$

For the purposes of solar activity reconstruction, the best archive for atmospheric ^{14}C measurement are tree rings, measured at single year e.g. (Miyake et al. 2012) and decadal e.g. (Stuiver & Becker 1993) time scales. However due to its long atmospheric residence and complex lifecycle within the Earth system, the measured ^{14}C in tree rings is not a direct reflection of the ^{14}C production rate, but a time-shifted and dampened version of it. This suppression and time-shift can be corrected using a reversed carbon cycle model which accounts for ^{14}C in multiple reservoirs and calculates the actual ^{14}C production rate (Muscheler 2000).

2.3.2 Beryllium-10

Beryllium-10, which is formed through spallation of atmospheric oxygen and nitrogen, has a larger half-life (approx. 1.386 ma; Chmeleff et al. (2010)) compared to ^{14}C. It is more rapidly scavenged from the atmosphere as it readily binds to aerosols. These aerosols combine with water droplets and precipitate on the Earth's surface - the dominant deposition process referred to as wet deposition (Lal & Peters 1967). Regions which receive a higher amount of precipitation, for example the tropics and coastal areas in polar regions, will in turn receive the highest flux of ^{10}Be through rapid atmospheric scavenging of ^{10}Be and wet deposition. Relative ^{10}Be flux is also dependent on where stratospheric-produced ^{10}Be enters the troposphere, which is mainly at mid-latitudes (fig. 5).

These factors need to be considered when reconstructing global ^{10}Be production/deposition rates. Regardless, Heikkilä & Smith (2013) have shown that, in general, ^{10}Be records are well suited as solar activity proxies. Where precipitation is scarce, such as Antarctica, ^{10}Be is mainly deposited through so-called "dry deposition" via gravitational settling processes.

The reduced atmospheric residence time of ^{10}Be, relative to ^{14}C, results in a more direct signal of production rate within annual archives such as ice sheets. Beryllium-10 concentrations within geological archives are subject to climate influences, meaning they are not a direct reflection of incident cosmic ray flux, but are also influenced by atmospheric circulation and accumulation rate changes.

Berggren et al. (2009) use a calculation for deriving the deposition flux of ^{10}Be, which helps remove large ice-age scale variations in ^{10}Be concentrations in ice core archives. It remains unclear if this calculation leads to any correction or improvement of Holocene ^{10}Be production rate estimates.

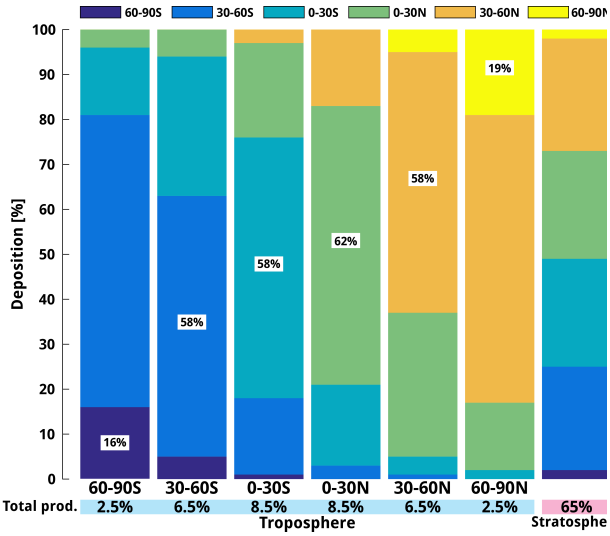

Fig. 5. Production (x-axis) and deposition (y-axis) of ^{10}Be as a percentage for given latitudes and atmospheric layers. Far right stack shows the dominant production of ^{10}Be in the stratosphere (65%), with deposition occurring semi-homogeneously between the mid latitudes. Troposphere-produced ^{10}Be is deposited heterogeneously. For example: ^{10}Be produced in the troposphere between 60-90°S is deposited to 16% between 60-90°S, to 65% between 30-60°S and to 15% between 0-30°S (left most stack). Deposition which occurs in the same latitudes as production are labelled. Figure modified from Heikkilä et al. (2009).

2.3.3 Chlorine-36

Chlorine-36 (half-life 301 ka; Beer et al. (2012)) is produced in the atmosphere through cosmic ray spallation of ^{40}Ar or through release of ^{36}Cl to the atmosphere from nuclear bomb tests (Synal et al. 1990). Because of the extremely low abundance of ^{36}Cl in the environment, double the amount of ice is needed compared to ^{10}Be for AMS (accelerator mass spectrometry) measurement. In addition, the current cost of measurement is very high, making it less commonly used in solar activity reconstructions compared to ^{10}Be and ^{14}C.

Cosmogenic ^{36}Cl production mainly occurs in the stratosphere (~54-90%; Huggle et al. (1996); Masarik & Beer (1999)). Stratospheric-produced ^{36}Cl is either bound to aerosols (such as $Na^{36}Cl$; Beer et al. (2012)) or more rarely form in a gaseous state ($H^{36}Cl$ / $^{36}Cl_2$). These aerosol-bound and gaseous forms of ^{36}Cl are transported out of the stratosphere and across the tropopause within ~2 years (Synal et al. (1990); Tosaki et al. (2012). They are then removed rapidly from the

troposphere through dry and wet deposition. Based on estimates of atmospheric aerosol residence times (Turekian et al. (1977); Bleichrodt (1978) and Raisbeck et al. (1981), the mean residence time of ^{36}Cl in the troposphere is expected to be several weeks.

Low natural concentrations mean that ^{36}Cl transport and deposition cycles are mostly derived through fallout of bomb produced ^{36}Cl (Synal et al. 1990), meaning no 'natural' ^{36}Cl cycle investigations have been made, limiting our understanding of transport and deposition changes across latitudes. As is the case with ^{10}Be, we can only assume that the concentrations of ^{36}Cl in ice cores are somewhat representative of atmospheric production rates, allowing us to investigate temporal variations. A known caveat of ice bound ^{36}Cl (as gaseous $H^{36}Cl$), is its inclination to become mobile post-deposition through upward diffusion. During snow metamorphism, the upper firn layers in the snow pack are subject to physical transformations which are thought to result in the release of gaseous species from snowflakes, including gaseous $H^{36}Cl$ (Delmas et al. (2004); Arnaud et al. (2000)). Some of this released $H^{36}Cl$ can then be redeposited on younger layers through co-condensation with water vapour. This upward mobility of $H^{36}Cl$ needs to be considered when using ^{36}Cl in ice for the purposes of solar activity reconstruction, particularly in low accumulation regions where dry deposition dominates, such as Antarctica.

2.4 Solar Proton Events (SPE)

It has recently been shown that solar proton events (SPEs) can act as a source for rapid increases in the production of cosmogenic radionuclides in the Earth's atmosphere (Mekhaldi et al. 2015). The same scenario may exist for the LU2610 and LU7510 events, therefore the main attributes of SPEs will be reviewed here.

Energetic events on the Sun's surface periodically result in large fluxes of high-energy solar protons directed at the Earth, with some studies suggesting they are more likely to occur near Solar Maximum (Shea & Smart 1990; Webb & Howard 1994; Gopalswamy et al. 2003). Such a period of elevated solar proton flux, generally lasting for a few days, is known as a solar proton event (Jackman et al. 2005). In the case where all particles and nuclides are considered, these events are referred to in the literature as solar particle events. A percentage of these accelerated solar protons have enough energy to penetrate the Earth's atmosphere, and are guided by the Earth's magnetic field - impacting both the northern and southern polar cap regions (>60° geomagnetic latitude) where geomagnetic cut off rigidities are lower.

The concept of an SPE and the measurement of its magnitude have been given many names in the ~60 years since its discovery. Mostly attributed with detection technique, these energetic events have been referred to as solar cosmic ray events, ground level events, polar cap absorption events and solar electron events (Shea & Smart 1990). The most extreme events are often referred to as ground level enhancements (GLE). GLEs are measured by neutron monitors at the Earth's surface and provide measurements in terms of neutron flux and, in some cases, energy distribution (Gordon et al. 2004). Neutron monitors only detect highly energetic secondary neutrons, and provide measurements in terms of percentage above the pre-event flux count. It should also be noted that neutron counters do not directly measure the primary cosmic rays, but the neutron by-product of the reactions initiated by them (Gordon et al. 2004). Orbital spacecraft and satellites, which are not hindered by the blocking effects of our atmosphere, are many orders more sensitive than Earth-based measurements to incoming energetic particles. Satellites such as the Geostationary Environmental Satellite 15 (GOES-15) can measure much lower energy particles and specific compositions of solar particle events at a wide energy spectrum, ranging from ~1 to ~100 MeV.

It is commonplace for SPEs to be detected in terms of their specific proton fluence spectra, which describes the flux of particles (protons) at varying energies per surface area, usually cm^{-2}. These spectra are generally defined as being either 'soft' or 'hard' depending on the kinetic energy distribution of the proton flux. Events which produce a higher than average flux of mainly low energy protons are usually categorised as soft, whereas hard SPE spectra show a relatively higher than average flux of protons with high and low energies. In both cases, it is conventional to describe the SPE intensity in terms of its fluence above 30 MeV or F (> 30 MeV) resulting in the standard F_{30} parameter. This convention is not without dispute, with some authors finding it ambiguous and strongly dependent on the assumed shape of the energy spectrum (Kovaltsov et al. 2014), however for the purposes of this study it will suffice.

A noteable hard SPE which has been recorded during the instrumental era occurred in February 1956, which was measured with a GLE peak of 5,500% above normal average, and estimated to have had an F_{30} of 1.8×10^{9} protons.cm^{-2} (Meyer et al. (1956); Webber et al. (2007)). An example of a soft SPE occurred in 1972, where a fluence of 4×10^{9} protons.cm^{-2} was recorded (Cane et al. (1986); Shea & Smart (1990)). Probably the most popular solar event, due to its extreme effects, such as wide spread telegraph system outages over Europe and North America, is the Carrington event which occurred prior to instrumental measurement in September of 1859. Proposed to be an extreme solar flare, the event was well documented in terms of purely observational data at the time (Shea & Smart 2006), however subsequent studies have attempted to reconstruct the event empirically to allow comparisons with modern day solar proton events.

McCracken (2001) performed such a reconstruction by using nitrate concentrations in polar ice archives to calculate an F_{30} value of $\sim1.9\times10^{10}$ protons.cm^{-2}. Smart et al. (2006) found an absence of increased ^{10}Be in different ice cores for the same period, drawing the conclusion that the Carrington event was of a soft spectrum, with a high proton flux of lower energies. Agreement on this reconstruction is not unanimous however, with some authors unable to find the same nitrate concentration spike in other ice cores for the same period (Wolff et al. 2012), and

hence were unable to reach the same conclusions. The fact that nitrate enhancements can at all be attributed to solar flares is heavily disputed, with some authors stating that such nitrate spikes can be produced due to enhanced deposition (Wolff et al. 2008).

A recent study by Mekhaldi et al. (2015) used annually resolved ^{10}Be measurements from several ice cores to confirm a solar source for a large spike in atmospheric radiocarbon (^{14}C) around AD 774/5 and 993/4. The authors concluded that the AD 774/5 event most likely had an F_{30} well above 10^{10} protons.cm^{-2} - about 5 times larger than any SPE observed during the instrumental period between 1956 and 2005. The identification of such events in the geological record is the motivation for the current study, with the aim of such studies to better constrain the frequency of such severe solar events.

3 Methods and Dataset

The goal of this study is to investigate a source for the previously mentioned rapid changes in ^{14}C found in the IntCal13 dataset (LU2610 and LU7510 events). Existing ice core records of ^{10}Be and ^{36}Cl have been investigated, and new measurements have also been made, all of which are described in the following section.

3.1 Existing Datasets

The IntCal13 calibration curve, which was used to locate the two potential events for this study, utilises radiocarbon (^{14}C) measurements from tree rings and provides a continuous record of Δ^{14}C fluctuations throughout the Holocene. The mixed decadal and single year measurements which form the smooth IntCal13 curve makes it unsuitable for quantifying potential spikes in ^{14}C against background production, and therefore unsuitable for comparing the magnitude of these spikes against short temporal variations in other radionuclides such as ^{10}Be and ^{36}Cl. It would be preferable to use annual or biannual ^{14}C measurements for such a comparison.

Although many ice core records have been accumulated over the past several decades, the measurement of cosmogenic radionuclides such as ^{10}Be and ^{36}Cl have been intermittent and sparse; usually at varying resolutions and time spans. Generally, aside from ^{36}Cl, an annual or biannual resolution of cosmogenic radionuclide measurement is required to confidently investigate the occurrence of large SPEs.

In the case of ^{36}Cl, the resolution of measurement is generally lower due to lower natural concentrations. However, the sensitivity of ^{36}Cl production to low energy particles mean that these measurements are still useful for solar activity reconstructions. For some periods during the Holocene ^{36}Cl measurements are available for the GRIP ice core at ~5.5 yearly resolution (Wagner et al. 2000). In the case of ^{36}Cl, two samples were combined to produce a single measurement due to low natural ^{36}Cl concentrations, resulting in the lower resolution record. The record is not continuous for the entire core, however the LU2610 interval relating to this study has been partially measured. No comparable radionuclide records for the LU2610 and LU7510 intervals in the southern hemisphere (i.e. Antarctica) have been published at time of writing, meaning a global signal for the two events in question cannot currently be analysed. An itemisation of the datasets used in this study are shown in table 1.

3.2 GRIP ^{36}Cl

Existing concentrations of ^{36}Cl within the GRIP core (geographical location shown in fig. 6) have been measured at a resolution of ~5.5 years for the period covering LU2610, however no ^{36}Cl records exist for the LU7510 period. In order to establish a reliable radionuclide flux, the accumulation rate needs to be known for the corresponding period of the radionuclide data. Accumulation rate within an ice core is usually established through layer counting, whereby the number of layers within a given section will represent the number of years of deposition. In response to the overlying weight of the ice sheet, there is thinning of layers at greater depths due to strain. If one was to simply estimate (via layer counting) the thickness per year at these depths, the accumulation rate would appear to decrease almost exponentially. Therefore, a strain model is used to correct for this 'thinning' effect. Once the strain has been modelled for a given depth, it can be used to reverse this thinning effect. Additionally, the existing GRIP time-scale has

Table 1. Itemisation of tree ring and ice core archives used in this study.

RECORD	SOURCE	PROXY	TIME SPAN (GICC05)	RESOLUTION (YEARS)	REFERENCE
INTCAL13	Tree rings	^{14}C	2595 – 2626 7499 - 7530	10	Reimer et al. (2013)
GRIP	Ice (Greenland)	^{36}Cl	2595 – 2626	~5.5	Wagner et al. (2000)
NGRIP	Ice (Greenland)	^{10}Be	2595 – 2626 7499 - 7530	~1 ~1	This study

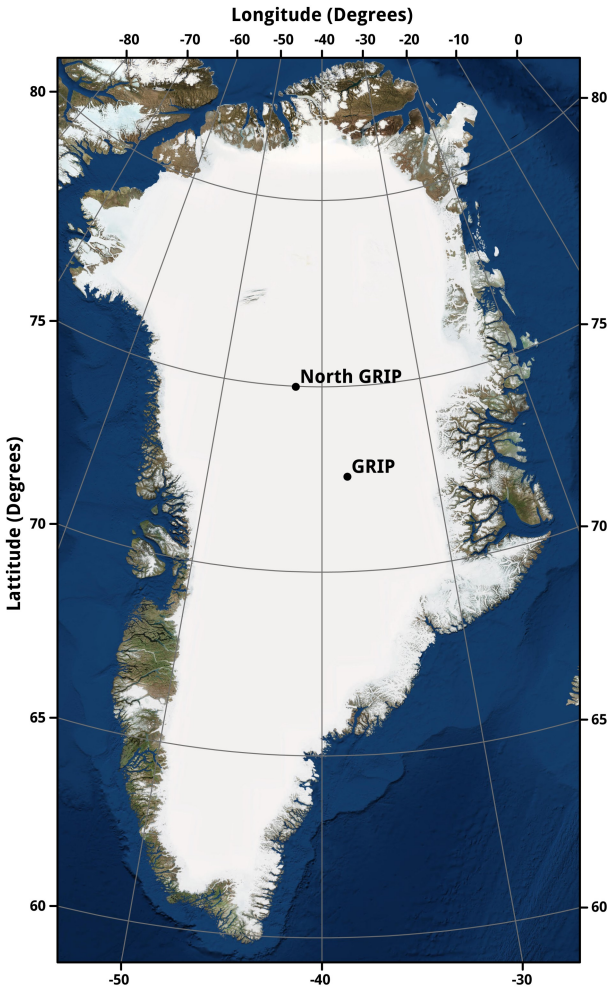

Fig. 6. Location of the two Greenland ice cores used in this study (Stauffer 1991; Gundestrup 2000)

been corrected according to the proposed IntCal13-GICC05 transfer function by Adolphi & Muscheler (2016). The resulting GRIP data is shown in figure 7.

3.3 New dataset: NGRIP ^{10}Be

In order to confidently investigate short-term solar events during LU2610 and LU7510, continuous high-resolution resolution records of ^{10}Be and ^{36}Cl are required. New sub-annually to annually resolved ^{10}Be measurements have been made for the corresponding sections of the NGRIP ice core (geographical location shown in fig. 6), with the process of sampling and measurement described below.

3.3.1 Ice sampling

A series of NGRIP ice core samples were obtained from the Centre for Ice and Climate in the Niels Bohr Institute of the University of Copenhagen, Denmark. During the initial drilling of NGRIP, the core was cut into ~55cm segments at the coring site. Annual layer thickness in the core at the proposed depths is approximately 11cm, therefore the segments were cut by band saw into 5 pieces (depending on segment length) within the core storage facility at the Centre for Ice and Climate, at an ambient temperature of -15°. Each of the resulting 78 samples was then bagged individually to avoid cross contamination and transported to the Cosmogenic Radionuclide laboratory at Geocentrum II in Lund University, Sweden for preparation for Accelerator Mass Spectrometry (AMS) measurements of ^{10}Be (and eventually ^{36}Cl).

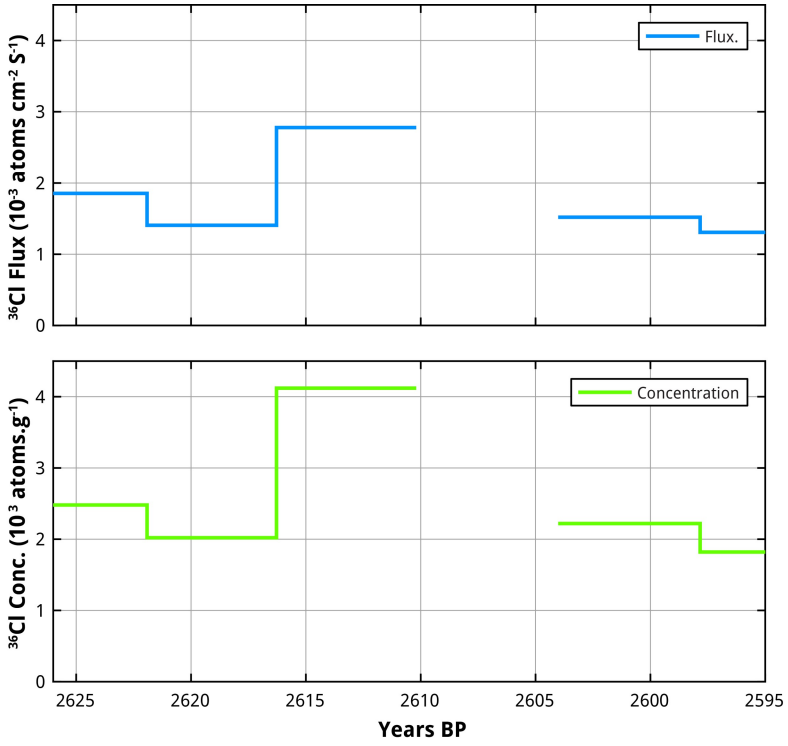

Fig. 7. Chlorine-36 concentration and calculated flux for the LU2610 period in the GRIP core (Wagner et al. 2000)

3.3.2 Chemical preparation for AMS measurements

The chemical preparation of ^{10}Be and ^{36}Cl for AMS measurements in this study follows the same procedure used by previous authors who have worked on this and similar ice cores (Berggren et al. 2009; Mekhaldi et al. 2015) and is described below:

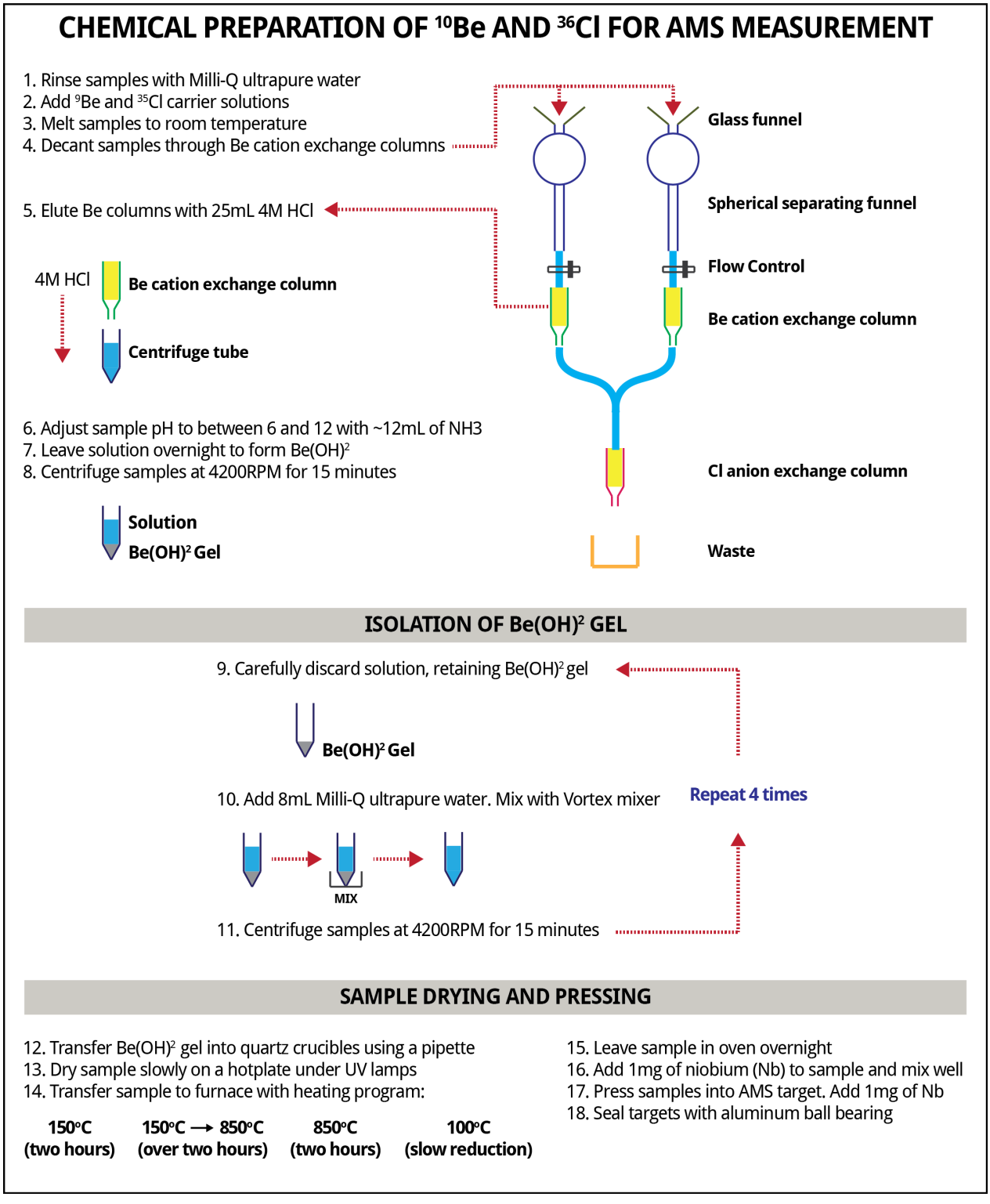

Firstly, the ice samples of 100-200g were cleaned with Milli-Q ultrapure water to eliminate any potential contaminates introduced during drilling or subsequent processing. Two carrier solutions were then precisely added to the samples via pipet: 0.1ml of 1000mg/l standard beryllium (^{9}Be-carrier) and 1ml of 1000mg/l Cl (^{35}Cl-carrier). Both carriers are required as part of the AMS procedure in order to calculate the amount of the rare radionuclide in each sample (^{10}Be and ^{36}Cl respectively). Adding these carriers as early as possible ensures that any subsequent loss of sample from this point on will not impact the overall ratio of isotopes within the samples. The ice samples where then sealed in pre-weighed and sterilised containers before being incrementally melted in a microwave oven. Care was taken to control the time of melting to avoid any boiling and/or sublimation.

The melted samples were then decanted into glass funnels which were linked to cation exchange columns (Bio-Rad Poly-Prep prefilled chromatography cation columns AG 50W-X8 resin 100-200 mesh hydrogen form 0.8x4) via silicon tubes which could be clamped to modulate flow. These cation exchange columns capture the beryllium (^{10}Be and ^{9}Be) from the melted ice, before allowing the water to flow onto the next column. Silicon tubes then directed the resulting water to a set of anion exchange columns, which were manually filled with Bio-Rad AG 4x4 resin (100-200 mesh free base form). This secondary set of anion columns are intended to capture Cl ions from the sample water, and were combined from two samples to increase the captured amount of Cl. Although not measured in this study, these samples have been stored in the Cosmogenic radionuclide laboratory at Geocentrum II in Lund University for later analysis. A series of 12 blanks consisting of Milli-Q water (~150g) were also processed in the same way to allow for an estimation and correction of any background contamination.

The beryllium resin columns were then mounted below sterilised funnels and eluted with a 25mL solution of 4M HCL. The resulting eluate, consisting of beryllium isotopes and HCL, was combined with 12mL of NH_3 in order to reach a pH of between 6 and 12, allowing for the formation of beryllium hydroxide ($Be(OH)_2$). The samples were then left in centrifuge tubes overnight to allow precipitation of $Be(OH)_2$, before being centrifuged at 4200 RPM for 15 minutes. The centrifuge processing separated a translucent Be $(OH)_2$ gel from solution. The solution was discarded, retaining only the $Be(OH)_2$ gel. Milli-Q water (8mL) was added to the gel and mixed thoroughly using a Vortex mixer before being centrifuged again for 15 minutes at 4200 RPM. The water was discarded and the process was repeated four times, until all that remained was a pure $Be(OH)_2$ gel (see lab schematic on previous page).

The $Be(OH)_2$ gel was then transferred into quartz crucibles using a pipette before being slowly dried on a hot plate under UV heat lamps. Once dry, the samples were transferred to a laboratory oven where a programed heating process was performed, heating the samples to 150°C for 2 hours before stepping up to 850°C over a period of two hours and maintaining 850°C for a further 2 hours. The temperature in the oven was then decreased gradually to approximately 100°C, and the samples remained in the oven overnight to prevent contact with air moisture. The samples, now a powder-like BeO, were left to cool. Once they had reached room temperature, about 1mg of niobium (Nb) was added to enhance AMS currents. The BeO was then well mixed with the Nb before being pressed into titanium cathodes (AMS targets). Once the pressing was complete, another 1mg of Nb was added before the cathode was sealed with an aluminium ball bearing. The resulting AMS targets were then shipped to Tandem Laboratory, University of Uppsala, Sweden for AMS measurement.

3.4 Data treatment and analysis

Galactic cosmic rays are responsible for much of cosmogenic radionuclide production in the Earth's atmosphere. The remaining production, which is much smaller by comparison, is due to solar cosmic rays. The impact of SCR on the production rate of ^{10}Be, ^{36}Cl and ^{14}C (along with others) have been extensively modelled (Webber et al. 2007; Usoskin & Kovaltsov 2008; Kovaltsov et al. 2012). Conclusions drawn from this modelling show that particularly large SPEs can contribute to the total yearly cosmogenic radionuclide production. Such an event occurred on February 23rd 1956, and, in the case of no latitudinal mixing, is estimated via modelling to have contributed about 40% of the total production of ^{10}Be above 65° latitude that year (Meyer et al. 1956; Webber et al. 2007).

In order to identify whether an SPE has impacted the production rate of cosmogenic radionuclides, we first need to establish the background GCR production rate for the period of investigation. This background rate of GCR-based production, once established, can then be used as a baseline for investigating possible peaks in production due to increased SCR. Additionally, if an increase in production relative to this baseline is determined, we need to know whether it can be explained by normal solar modulation or other factors not related to SCR. A common index of solar modulation is referred to as the solar modulation function (Φ), which is measured in MeV and varies from 0 (no solar modulation) to 2000 MeV (maximum solar modulation). Based on analysis of neutron-monitor data by Muscheler et al. (2016), a Φ range of 400 to 1400 MeV was used here to simulate minimum and maximum modulation parameter, which corresponds to approximately 0.0197 atoms cm^2 s^{-1} and 0.0104 atoms cm^2 s^{-1} respectively in terms of modelled globally averaged ^{10}Be production rate (Herbst 2013).

The background level for ^{10}Be measurements performed in this study will consist of a time weighted average of ^{10}Be production prior to and following any notable peaks within measured data. A similar method will be used to establish a background production for GRIP ^{36}Cl data.

Initially, the prospective peaks in radionuclide production were identified through analysis of the IntCal13 dataset. The main criteria for selecting a possible peak involved a rapid increase in ^{14}C, over annual timescales if possible (i.e. rapid changes from one year to the next). As seen in figure 1, the IntCal13

dataset for the periods of investigation invoke a composite of tree ring archives. The two periods of investigation show relatively strong ^{14}C increases in the low resolution data which could indicate short term events. However, quantifying these events against a background is difficult due to the low resolution of the IntCal13 dataset.

3.5 Radionuclide production and deposition fluxes

Radionuclide measurements in ice cores are recorded as the ratio of rare to common nuclide, i.e. $^{10}Be/^{9}Be$, before being transferred to the concentration of the rare nuclide (atoms per gram of ice, conventionally expressed as 10^4) when sample weight and carrier amount is known. An increase in snow accumulation for a given year may result in a dilution of radionuclides (Berggren et al. 2009). In order to correct for these 'amount' effects, ^{10}Be and ^{36}Cl fluxes were calculated using the following equation:

$$F = \frac{A * \rho_{ice} * C}{S} \quad (2)$$

Where A is the accumulation rate (cm/year), ρ_{ice} is the density of ice (g/cm^3), C is the concentration of radionuclides (atoms/g) and S is the number of seconds in a year. The resulting flux is expressed as atoms / cm^2 s^{-1}. In the case of ^{36}Cl measurements from the GRIP core, a strain model was used in conjuction with yearly layer thickness to calculate the change in yearly accumulation rate. For the new NGRIP ^{10}Be measurements, no strain model was available, therefore a fixed accumulation rate of 0.192 meters per year was used.

4 Results

4.1 NGRIP ^{10}Be measurements

New sub-annually to annually-resolved NGRIP ^{10}Be measurements from this study, although partially incomplete, span the periods BP 2595-2626 and BP 7499-7530 (fig. 8). These ages are based on the Greenland Ice Core Chronology 2005 (GICC05; Vinther et al. (2006)), and have been IntCal13-GICC05 transferred according to Adolphi & Muscheler (2016). In order to estimate the possible weather influences on the production signals of ^{10}Be (NGRIP) and ^{36}Cl (GRIP), the deposition flux for each record has been calculated using equation 2.

NGRIP ^{10}Be measurements (resolution ~0.96-1.1 years), for the period from 7499 - 7530 do not show a clear spike in ^{10}Be concentration, however there is a small increase at BP 7504, with a ^{10}Be concentration of 3.78 10^4 atoms.g (fig. 8 (a)). Concentration measurements directly prior to and after this increase vary from 2.09 to 2.1×10^4 atoms.g^{-1}, before increasing to 3.02 and 3.33×10^4 atoms.g^{-1} respectively. The younger period of measurement (resolution ~0.74-1.1 years), 2595 - 2626, shows a prominent peak in deposition at BP 2612, reaching ^{10}Be concentrations of 3.81×10^4 atoms.g. Concentration measurements directly prior to and after this peak are of a similar magnitude, indicating a peak span of ~2-3 years. This peak in ^{10}Be concentration has a close temporal match to the rapid change in ^{14}C seen in the IntCal13 dataset (fig. 1).

4.2 Production surplus

LU2610 Event: Once the deposition flux was calculated (see §3.5), the background level for the newly measured LU2610 NGRIP data was defined as the time weighted mean flux for the dataset excluding the (three) peak values; calculated to be 0.0090 atoms.cm^{-2} s^{-1}, with a peak deposition flux of 0.0212 atoms.cm^{-2} s^{-1} (figure 10). The relative flux increase occurs over a ~2-3 year period, however, excess cosmogenic radionuclide production due to SPEs is expected to occur contemporaneously with the initial event, with the exception of multiple events occurring over the same three-year period. Therefore, any lead and lag flux increases can be attributed to atmospheric residence time (~1-2 years for ^{10}Be; McHargue & Damon (1991); Masarik & Beer (1999)), deposition-related delay and/or multiple SPE events.

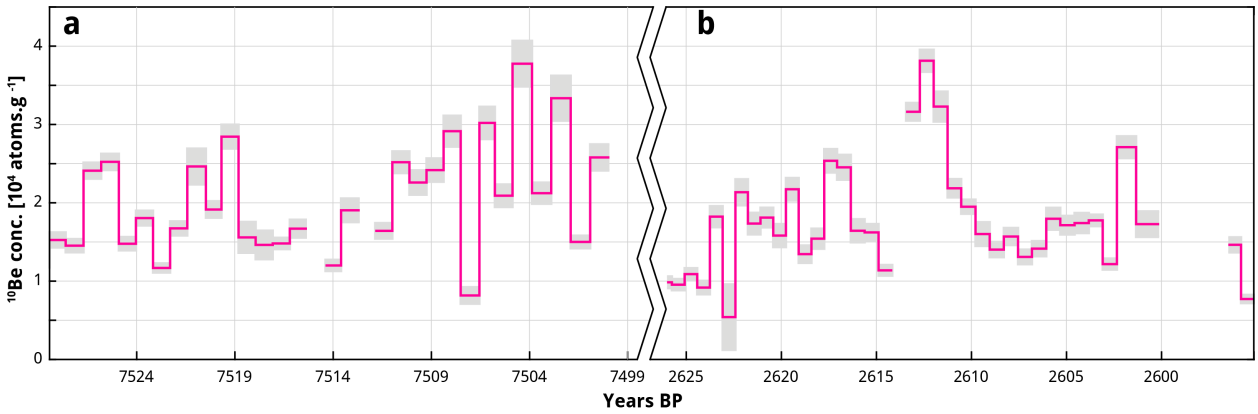

Fig. 8. Measured NGRIP ^{10}Be concentrations. Shading represents upper and lower measurement error. A timescale break has been placed at 2595-7530.

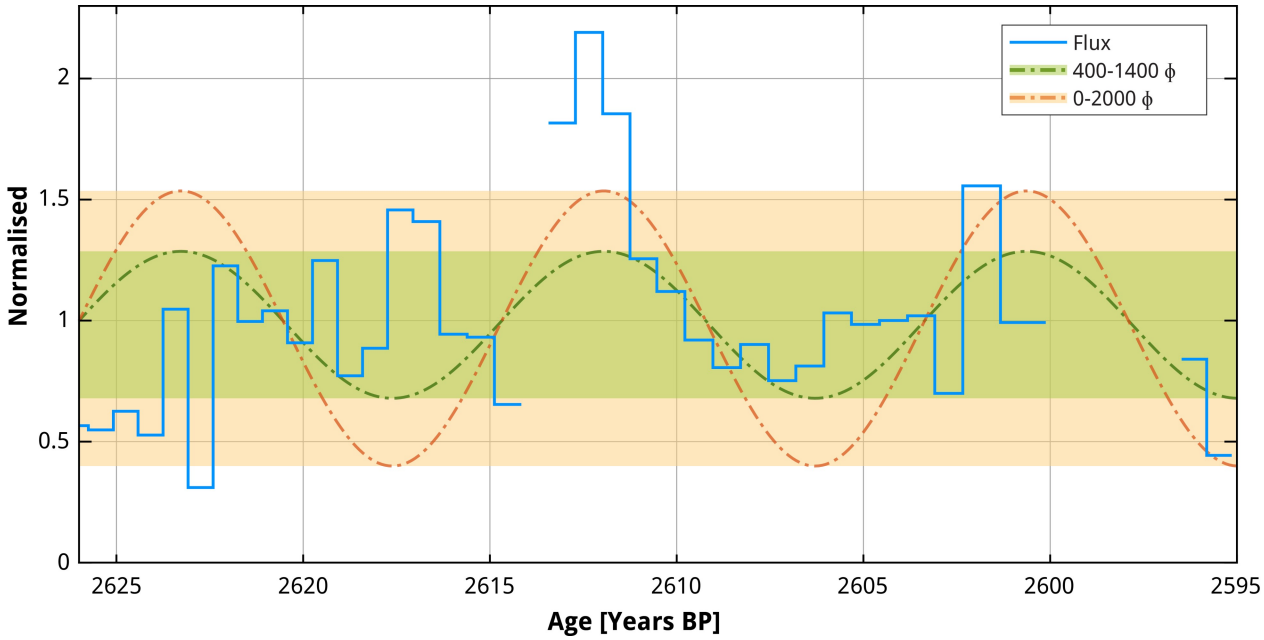

Fig. 9. Calculated ^{10}Be flux from new NGRIP measurements for the LU2610 period. Calculated ^{10}Be flux has been compared against two ~11 year sinewaves used to simulate expected 'normal' solar modulation (400-1400 Φ, §3.4), and 0-2000 Φ, representing extreme minimum and maximum solar modulation. Corresponding bands have been applied to represent the vertical extent of the sine waves for the period. The flux and corresponding sine wave functions have been divided against their respective mean values in order to normalise the data for comparison.

By assuming that the excess production occurred due to a single event, the ~3 years which contain the peak in question have been integrated into a single year, resulting in a peak factor increase of 2.40 ± 0.11. This integration implies that, during one year, the ^{10}Be production increased by 240% relative to the background average. It should be mentioned that the new measurements (excluding peak values) all fall within the production range expected due to normal solar modulation (modulation explained in §3.4).

Qualitatively, there appears to be a sinusoidal variation in the dataset which may occur due to the 11-year solar cycle (Beer 2000). An attempt has been made to visually align an 11 year sine wave function to this cyclicity, with the peak occurring during a phase of solar minimum. In addition, corresponding bands of production due to solar modulation have been shown on figure 9, illustrating both expected production due to normal modulation (400 to 1400 MeV, figure 9), along with extreme minimum and maximum modulation parameters (0 to 2000 MeV).

Depositional flux also was calculated for ^{36}Cl concentration measurements in the GRIP core. Due to a lower resolution dataset (~5.5 years), a 200-year time weighted average (excluding peak values) was used for estimating the average ^{36}Cl deposition (BP 2500-2700); resulting in a background flux of 0.0016 atoms.cm^{-2} s^{-1}. A longer-term view of the GRIP core (fig. 10(e)) shows that the peak values being investigated sit well outside the average for the given period of interest, adding confidence to the estimated background value used here. It's worth considering that the relative increases in ^{36}Cl flux may be the result of measurement error, contaminated samples or post-depositional effects, however their temporal synchronicity with the ^{10}Be peak in the separate NGRIP core strengthens the theory of an overall peak in radionuclide production for this period. As seen in figure 10(c), the low-resolution measurement of ^{36}Cl in the GRIP ice core shows a peak of 0.0027 atoms.cm $^{-2}$ s^{-1} over a period of ~6 years. Once integrated into a single year, the peak represents a factor increase of 4.57 ± 0.22 relative to the calculated background average.

LU7510 Event: The apparent production rate change seen in the IntCal13 dataset for the LU7510 period is not clearly matched in the corresponding NGRIP ^{10}Be measurements. Although there are some deviations from the time weighted mean flux of 0.0113 atoms.cm^{-2} s^{-1}, there is no singular rapid increase at the annual scale which is independent of other peaks of similar amplitude (fig. 11). The dataset appears to contain abundant noise and there is generally no clear pattern, aside from a slightly increasing production towards younger parts of the record.

Summary of results for LU2610		
Radionuclide	^{10}Be	^{36}Cl
Peak factor (Flux)	2.40 ± 0.11	4.57 ± 0.22
Integrated flux enhancement (atoms.cm^{-2} s^{-1})	2.17 ± 0.02 x 10 $^{-2}$	7.2 ± 0.2 x 10 $^{-3}$

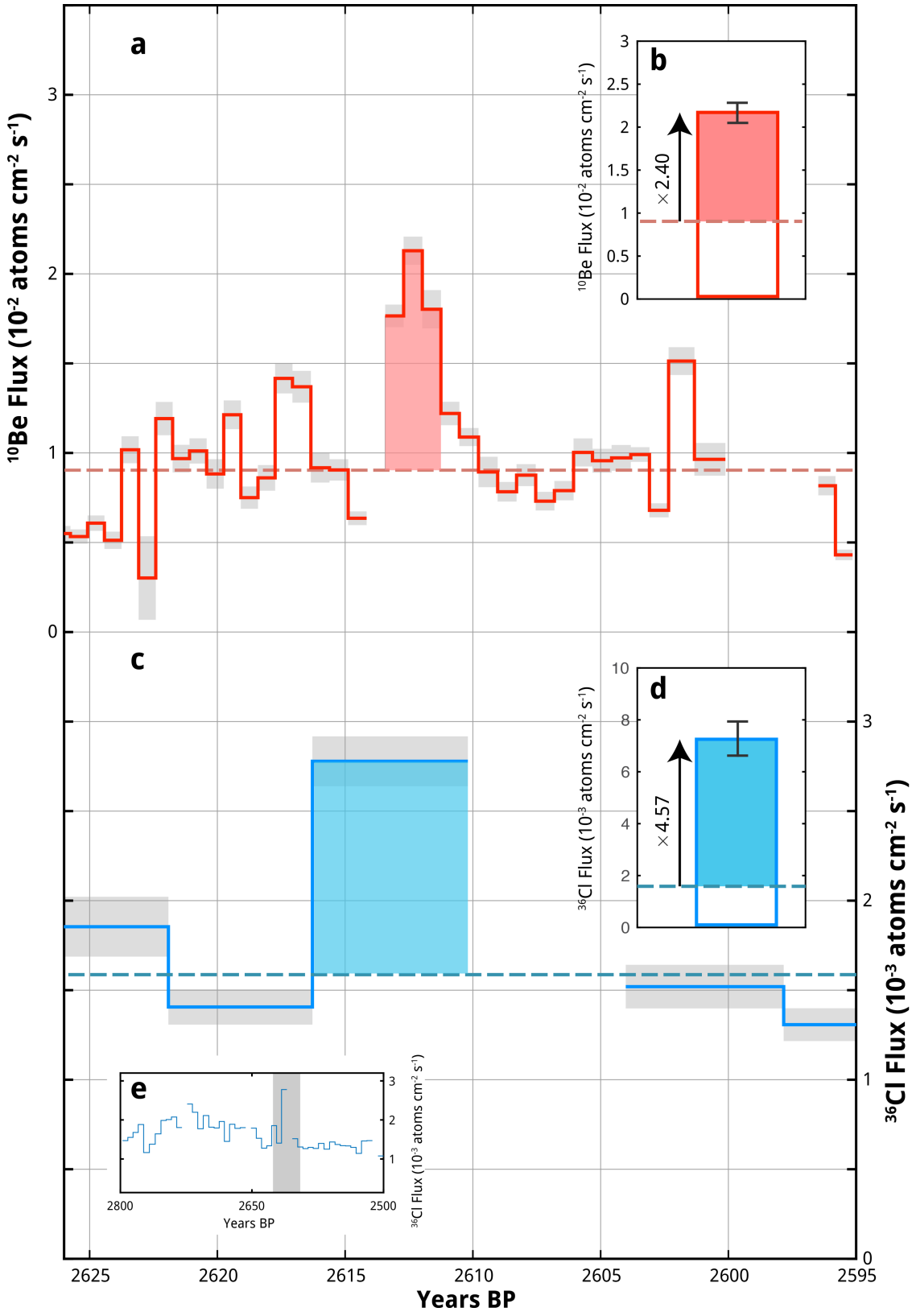

Fig. 10. ***LU2610 event view of ^{10}Be and ^{36}Cl.*** ***(a)*** *Time series for newly measured NGRIP ^{10}Be flux (red line), along with corresponding measurement error margins (grey shading).* ***(c)*** *Time series for existing ^{36}Cl GRIP measurements, displayed as flux (blue line). Filled areas represent estimated production enhancements relative to background production (dashed lines). Inset* ***(e)*** *is an extended time series for ^{36}Cl flux in the GRIP core, with the investigated period shown in grey. Sub figures* ***(b)*** *and* ***(d)*** *show radionuclide production enhancement fluxes in atoms cm^{-2} s^{-1} for the LU2610 event, integrated into 1 year for ^{10}Be and ^{36}Cl respectively. The radionuclide increases are indicated with arrows relating to the ratio between the inferred flux/production enhancements stacked over 1 year (filled rectangles) and estimated background levels (white rectangles). Error bars represent measurement uncertainty for the period of integration.*

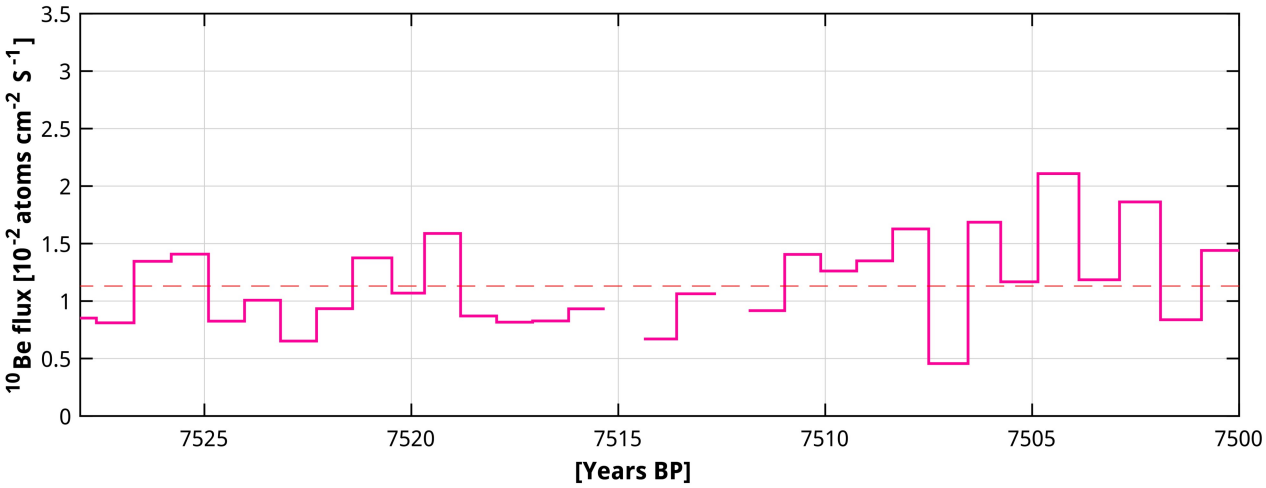

Fig. 11. Newly measured NGRIP 10Be measurements, displayed as calculated fluxes, for the LU7510 period. Estimated background flux shown as dashed line.

In summary, new and existing radionuclide measurements have been investigated for the LU7510 and LU2610 periods. A lack of additional existing radionuclide data for LU7510, along with no discernible peak in ^{10}Be production based on new measurements mean we are unable to draw conclusions on the possibility of a significant increase in radionuclide production for this period.

New ^{10}Be measurements for the LU2610 event indicate a flux 240% that of calculated background for a single year, which is synchronous with the rapid Δ^{14}C change found in the IntCal13 dataset. Additionally, previous measurements of ^{36}Cl in the GRIP core show a single year production increase of 457% for the LU2610 period.

5 Discussion

5.1 Assessing the cause of the LU2610 Event

The rapid change in Δ^{14}C seen in the IntCal13 dataset around 2610 BP (LU2610) and 7510 BP (LU7510), which prompted this study, have resulted in new NGRIP ^{10}Be measurements.

In the case of LU2610, these new measurements indicate an enhancement in ^{10}Be deposition (relative to background) which lasts for approximately 3 years. Further investigation has led to the discovery of a deposition enhancement (relative to background) in ^{36}Cl within the GRIP core, which is synchronous with both the rapid change in Δ^{14}C and the enhancement in NGRIP ^{10}Be.

The new NGRIP ^{10}Be measurements for LU7510 may indicate a minor ^{10}Be deposition increase towards younger parts of the record, with a minor peak in deposition relative to background around 7504BP. As this increase is only represented as a single data point, we are unable to distinguish it from noise in the dataset. Additionally, we currently lack published measurements for ^{10}Be and other radionuclides in different archives for this period. Considering currently available data, further conclusions on a radionuclide production increase for LU7510 will not be made here.

Instead, the remaining focus of this investigation will be on the LU2610 event, which is evidenced by short term radionuclide deposition enhancement from two separate ice core records and is possibly reflected in the IntCal13 dataset. The approach of the remaining investigation is to use this multiradionuclide record to define the source of said enhancement.

Although there is convincing evidence that past short-term increases in cosmogenic radionuclide production can in some cases be attributed to extreme solar proton events (Mekhaldi et al. 2015), it is not a foregone conclusion in the current study. However, as seen in §4.2 (fig. 9), the LU2610 radionuclide deposition enhancement, interpreted here as a short production increase, cannot be explained by solar modulation alone. Other possible sources of rapid short term increases in cosmogenic radionuclides include events such as relatively close supernovae and short gamma ray bursts (GRBs). These phenomena will be briefly investigated in respect to the LU2610 multiradionuclide enhancement to determine if they are possible and valid sources.

5.1.1 Long gamma-ray burst due to a recent and close supernova

Relatively close supernovae explosions, and the resulting gamma-ray emissions, have been suggested as possible sources for rapid increases in cosmogenic radionuclide production in the Earth's atmosphere, in particular ^{14}C and ^{10}Be (Damon et al. 1995; Brakenridge 2011).

Gamma-rays (γ -rays) which are produced during supernova explosions, and are unaffected by the geomagnetic or heliomagnetic fields, enter the atmosphere and generate atmospheric neutrons through photonuclear reactions (Zhou et al. 2013). These secondary neutrons can then react with atmospheric ^{14}N through ^{14}N(n,p)^{14}C (read 1 neutron + 1 ^{14}N atom gives 1 proton + 1 ^{14}C atom, see §2.2, fig. 3), resulting in production of ^{14}C. If we could quantify the relative increase of ^{14}C generated during the LU2610 event, we may be able to model the necessary incident γ-ray energy required to reproduce it. However, the relative ^{14}C in-

crease is unknown at this time, and outside the scope of this study.

Instead, we will compare the LU2610 event to AD775, an event which has a similar magnitude in terms of ^{36}Cl and ^{10}Be enhancement (fig. 11), and has a Δ^{14}C enhancement in of ~12‰ from one year to the other. Miyake et al. (2012) report no detectable increase in ^{14}C corresponding to supernovae SN 1006 and SN 1054 (Burrows 2000), and that the energy released during a supernova which corresponds to AD775 would have to be larger than these. The authors go on to calculate that a supernova which could be responsible for the AD775 event would need to have been ~2 kpc (65,000 lightyears) from Earth when they considered the typical γ-rays emissions by such an event (~3 10^{51} erg). Finally, although the authors cannot rule out an undiscovered supernova remnant corresponding to the AD 775 event, they state that such a supernova (occurring relatively recently and relatively close to Earth) would have resulted in a very bright x-ray and radio wave signature, the remnants of which would still be readily detectable with modern instruments.

Citing a similar radionuclide enhancement between the AD775 and LU2610 events, much of the same reasoning can be applied, advocating against the likelihood of a supernova source for LU2610. Therefore, unless a remnant is discovered which can match the required criteria to produce LU2610, we can rule out a supernova source at this time.

5.1.2 Short gamma-ray burst source

Short duration (<2 s) gamma-ray bursts (GRB) have been previously cited as a possible source for rapid increases in the production of cosmogenic radionuclides, specifically ^{14}C and ^{10}Be (Hambaryan & Neuhäuser 2013). Short GRBs, as opposed to longer bursts (Kouveliotou et al. 1993), emit more energetic photons and are thought to result from the coalescence of compact binary systems such as double neutron stars or neutron stars and black holes (Nakar 2007).

Although the conclusions from Hambaryan & Neuhäuser (2013) have since been proven spurious based on the use of unsuitable modelling data (Melott & Thomas 2012; Mekhaldi 2014), other authors have argued in favour of short GRBs as sources of rapid radionuclide enhancement. For example, Pavlov et al. (2013) attempted to predict the production of multiple radionuclides though the modelling of photonuclear reactions of primary cosmic rays (and their subsequent secondary particle cascades) with atmospheric atoms.

The resulting photon yield functions for direct photon-atom interactions are shown in figure 13. The authors show that high-energy γ-rays (E ~1-30MeV), do not result in a measureable ^{10}Be production increase for direct photon-atom interactions. According to the authors this is because the energy range of the cascade produced secondary particles (neutrons) is below the ^{10}Be spallation threshold (n ~15-20 MeV).

The ^{36}Cl spallation threshold for reactions on ^{40}Ar is approximately the same as ^{10}Be, however the spallation threshold for the ^{36}Ar(n,p)^{36}Cl reaction is much lower (neutron energy ~0.5MeV), meaning secondary particles with energy n ~ 1 MeV will efficiently produce ^{36}Cl via this reaction pathway without any accompanying ^{10}Be production. The significant production of ^{36}Cl via this pathway is dubious, considering the rarity of ^{36}Ar (^{40}Ar/^{36}Ar = 298.73 ± 0.28; Lee et al. (2006)). Nevertheless, the authors refer to this feature as the 'isotopic footprint' of short-GRB's, resulting in production increases of ^{14}C and ^{36}Cl, with the absence of ^{10}Be.

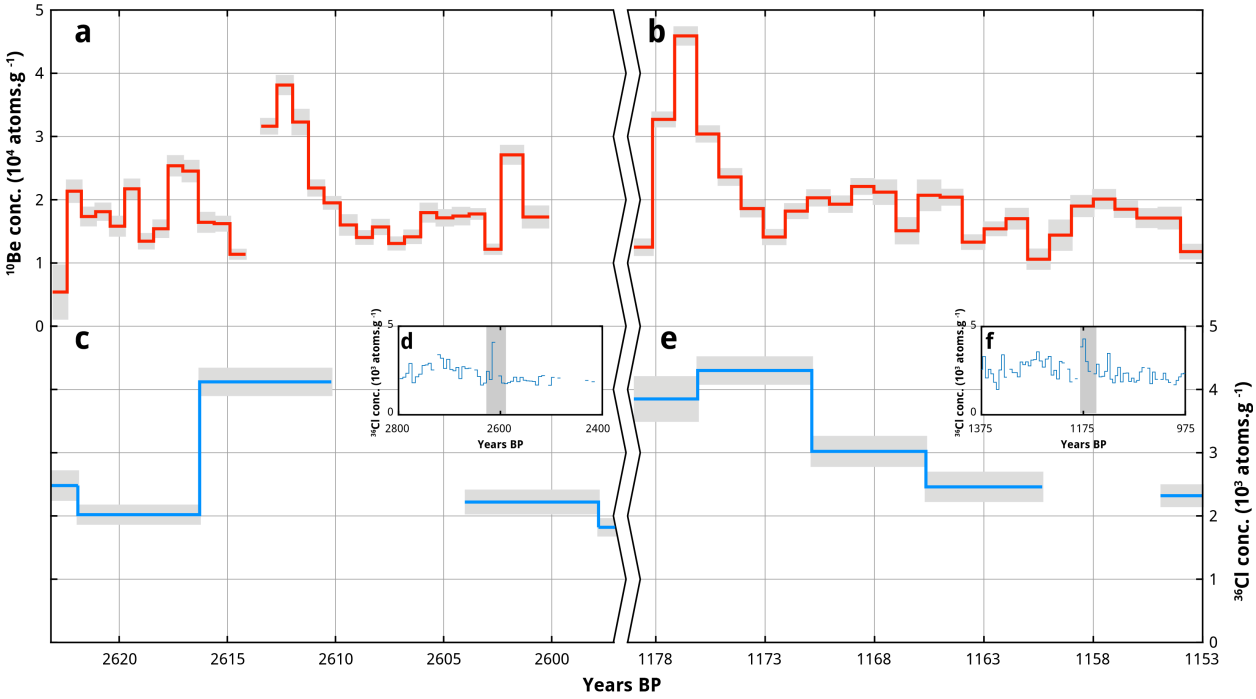

*Fig. 11. Comparison of LU2610 (**a**,**c**) and AD775 (**b**,**e**) radionuclide enhancements for NGRIP ^{10}Be and GRIP ^{36}Cl. Thick lines represent concentrations, with grey shading representing measurement error. Inset plots d and f extended time series for ^{36}Cl concentration. Note slightly higher ^{10}Be resolution measurement for LU2610, and the added time break between events.*

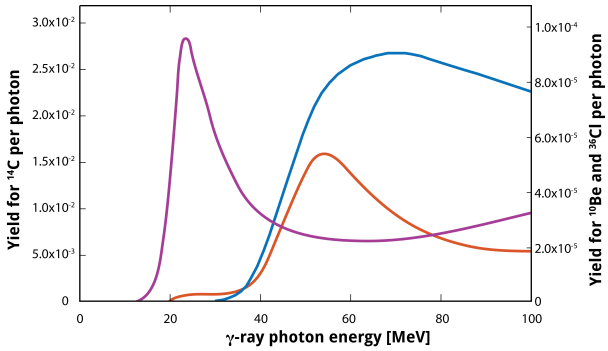

Fig. 13. Yield functions for direct γ-ray-atom interactions for ^{14}C (magenta), ^{10}Be (blue) and ^{36}Cl (orange). Modified from Pavlov et al., 2013.

Finally, Pavlov et al. (2013) state that short-GRB induced radiation would result in strong ionization of the atmosphere. This ionization would yield significant amounts of nitric oxides (NO*x*), a known catalyst of ozone depletion, in the stratosphere. The resulting ozone depletion would then lead to a rise of the tropopause, facilitating and accelerating stratosphere-troposphere exchanges. The authors hypothesize that the deposition rate of ^{10}Be could therefore increase, despite production remaining constant, due to a sustained injection of stratospheric air into the troposphere. Citing differences in stratosphere-troposphere based deposition between the arctic and Antarctic regions, the authors conclude that increased deposition of ^{10}Be due to sustained injection of stratospheric air into the troposphere would be more apparent in Antarctic ice records, resulting in a bi-polar asymmetry of ^{10}Be deposition.

More concisely, Pavlov et al. (2013) suggest that radionuclide evidence of a typical short-GRB would consist of a measureable excess of ^{14}C and ^{36}Cl, and possibly ^{10}Be in the Antarctic region, with an absence of arctic ^{10}Be depositional enhancement.

The new NGRIP ^{10}Be measurements for the LU2610 are interpreted to indicate a rapid production excess in ^{10}Be (fig. 10(a)) in Greenland. Although we are unable to directly compare the relative excess production in ^{14}C with ^{10}Be, the fact that a production excess occurs at all in the arctic is incompatible with mechanisms proposed by Pavlov et al. (2013). Therefore, a short-GRB is inconsistent as a source for the multiradionuclide enhancement for the LU2610 event based on currently proposed theories.

5.1.3 Solar proton event source

As outlined in previous sections, changes in solar modulation (see §4.2), supernovae and short-GRB's have been effectively eliminated (based on current data) as potential sources for the LU2610 event. We will now consider the remaining possible source: a solar proton event (SPE).

A solar source has been discarded by previous authors for other events with similar radionuclide enhancements, such as the AD775 event (Miyake et al. 2012; Hambaryan & Neuhäuser 2013). The main reasoning for the initial discarding of a solar source for the AD775 event was based on an overestimated ^{14}C production rate used by Miyake et al. (2012). Revisions to this production rate by subsequent authors (Melott & Thomas 2012; Usoskin et al. 2013) have indicated that a very strong SPE could have indeed been the source for AD775. Further to this, Mekhaldi et al. (2015) has also made a very compelling argument in favour of an SPE source for the AD775 event through a comprehensive multiradionuclide analysis.

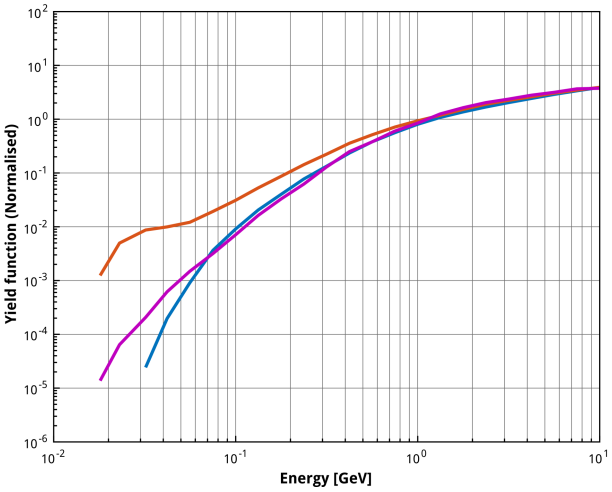

Fig. 14. Yield functions by protons for ^{14}C (magenta), ^{10}Be (blue) and ^{36}Cl (orange), divided by their respective mean values for comparison. Sources: ^{14}C (Castagnoli & Lal 1980), ^{36}Cl and ^{10}Be (Webber et al. 2007)

Although the excess of ^{14}C has not been quantified for LU2610, the enhancement in ^{10}Be and ^{36}Cl matches the expected production increase due to solar protons. When the yield functions of the three cosmogenic radionuclides are divided by their respective means (fig. 14), we can see that ^{36}Cl is relatively more affected by lower energy solar protons (~25-30MeV) compared to the other radionuclides. The results from this study show that the production excess of ^{36}Cl during the LU2610 event was increased by a factor of 1.9 compared to ^{10}Be, adding support for a solar source in terms of expected proton energy ranges. Finally, as opposed to the previously discussed short-GRB 'isotopic footprint' suggested by Pavlov et al. (2013), computations by Webber et al. (2007) show that the increased productions of both ^{36}Cl and ^{10}Be are theoretically a distinguishing feature of strong SPEs.

In summary, the new NGRIP ^{10}Be measurements from this study suggest a cosmogenic radionuclide enhancement event which is inconsistent with a supernova or short-GRB source for the LU2610 event, based on current data. The contemporaneous enhancement in GRIP ^{36}Cl, which is 190% that of NGRIP ^{10}Be, supports the hypothesis that an extreme solar proton event was the source of the LU2610 radionuclide enhancement. This hypothesis is further strengthened when we consider that: a) the radionuclide peaks in the LU2610 and AD775 events are similar in magnitude, b) it has been shown conclusively that the AD775 event is the result of a strong SPE and c) the alternative GRB source cited for both events are thought to occur much less frequently compared to energetic solar events (e.g. 1 GRB directed at Earth every 125,000 years (Melott & Thomas 2011)).

5.2 Parameters of LU2610 solar proton event

Galactic cosmic rays, which have on average much higher kinetic energies than solar particles, account for most cosmogenic nuclide production in the Earth's atmosphere (Beer et al. 2012). If we consider that the pronounced radionuclide enhancement recorded during the LU2610 event was the result of solar protons (e.g. a solar flare), the event in question must have been extraordinarily strong.

When also considered that a similar source has been proposed for the AD775 event (Mekhaldi et al. 2015), the periodicity of such strong events may be more frequent than previously thought (Usoskin & Kovaltsov 2012). It should be noted that such frequency estimates are based on very few controversially defined (Wolff et al. 2008) extreme solar events, and that some of the strongest instrumentally recorded events considered (e.g. SPE56) did not result in a large excess in ^{10}Be flux.

To better understand the periodicity and implications of extreme solar events, an attempt will be made here to describe the energy spectrum and fluence of the SPE source for LU2610.

5.2.1 The energy spectrum

The varying production yields of cosmogenic radionuclides are dependent on the energy spectrum of the source SPE. This means that a hard SPE with a smaller F_{30} (F_{30}; term explained in §2.4) than a soft SPE may result in the same cosmogenic radionuclide production. This feature has been exemplified though the computation of ^{10}Be and ^{36}Cl productions of historical SPEs from 1940 to 2005 (fig. 15) by Webber et al. (2007). The computations show that the very hard SPE of January 2005 (SPE05), which had an F_{30} of 2.0×10^{8} protons.cm^{-2}, produced as much ^{10}Be as the SPE of August 1972 (SPE72), which is considered as very soft, and had a much larger F_{30} of 4.0×10^{9} protons.cm^{-2}. In the same study, Webber et al. (2007) show that the hardest recorded SPE, February 1956 (SPE56), with a GLE (GLE; term explained in §2.4) of 5,500% and $F_{30} = 1.8\times10^{9}$, yielded 5 times more ^{10}Be than the soft event SPE72 which had an F_{30} over twice that of SPE56.

In terms of relative ^{36}Cl production, we see an inverse relationship, indicating that the production of ^{10}Be and ^{36}Cl is distinctive in terms of peak response energies. We can use this distinction to estimate the energy spectrum of the SPE related to LU2610 by

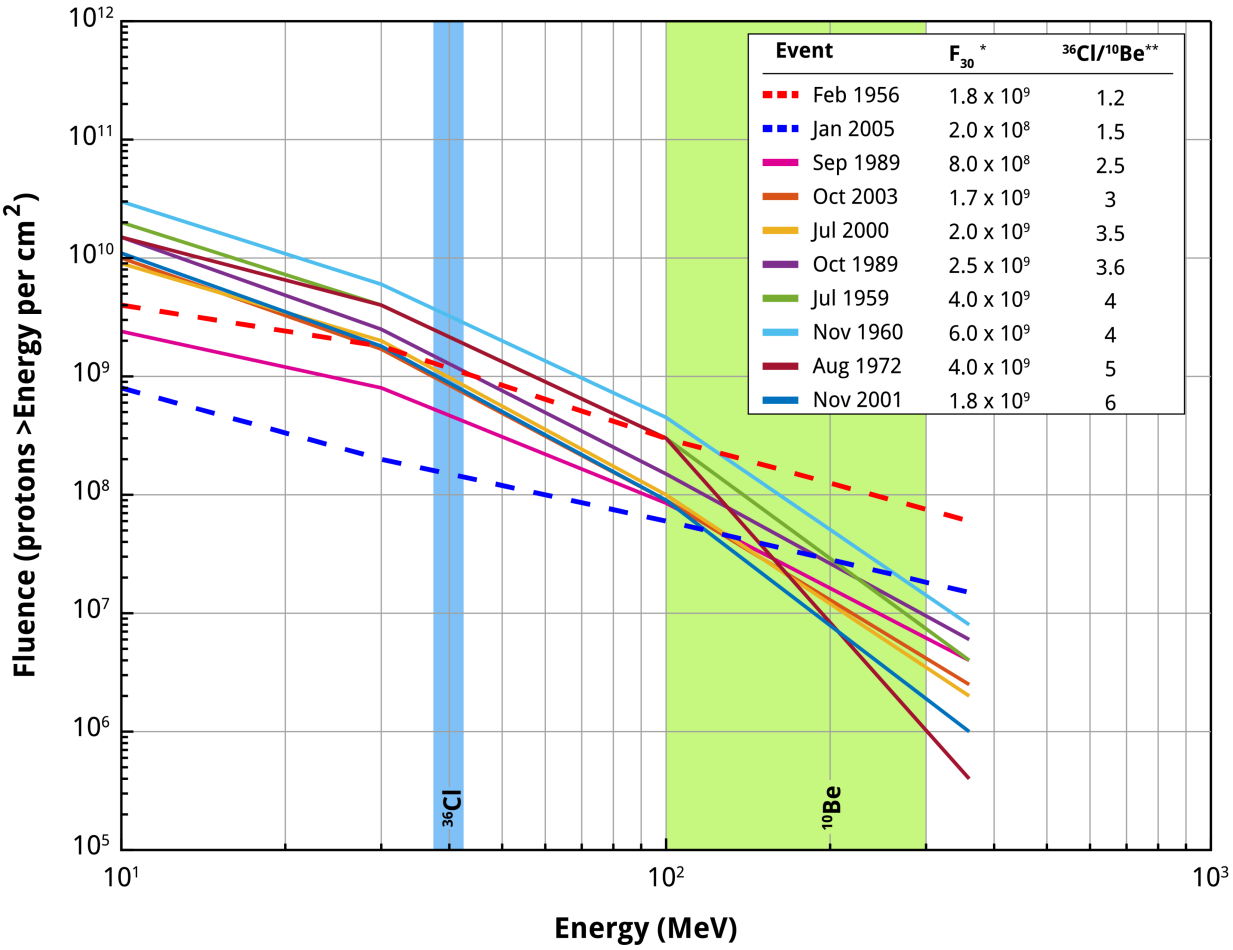

*Fig. 15. Event-integrated fluence spectra for 10 instrumentally recorded historical solar proton events occurring between 1956 and 2005 (Webber et al. 2007). Inset table shows corresponding event with F_{30} (*unit: protons.cm^{-2}) and ^{36}Cl/^{10}Be ratio (** relative ratios, after Mekhaldi et al. (2015)) . The blue and green bands indicate estimated specific peak response energies of ^{36}Cl and ^{10}Be (incident proton energies at which each radionuclide is predominantly produced). The blue and red dashed curves indicate very hard energy spectra SPEs. Modified from Webber et al. (2007) and Mekhaldi et al. (2015).*

comparing its relative $^{36}Cl/^{10}Be$ enhancement ratio to historical SPEs.

The integral spectra for major SPEs as calculated by Webber et al. (2007) are shown in figure 15 along with associated $^{36}Cl/^{10}Be$ ratios corresponding to the events (Webber et al. 2007; Mekhaldi et al. 2015). There is a clear relationship between the shape of the spectra and its associated $^{36}Cl/^{10}Be$ ratio which define the events into two distinct energy spectra groups: soft and hard. Hard SPEs, such as SPE56 and SPE05 tend to have increased production ratios < 2, while softer SPEs exhibit ratios > 3. The LU2610 event is calculated to have a $^{36}Cl/^{10}Be$ ratio of 1.90 ± 0.06. Based on this ratio, and its corresponding uncertainty, we can see that the event produced less than 2 times more ^{36}Cl than ^{10}Be. This places the LU2610 event into the hard spectrum category of solar proton events, with its most similar historical counterpart being SPE05, which had an $F_{30} = 2.0\times10^{8}$.

5.2.2 The fluence

The computations by (Webber et al. 2007) infer that SPE05 resulted in annual ^{10}Be production increase of about 2.4%. This ^{10}Be production increase assumes that global atmospheric mixing has taken place before deposition, as opposed to the case of no latitudinal mixing. The assumed scenario of global atmospheric mixing is more credible than no mixing, considering that the energy ranges of incident protons from SPEs would result in mostly stratospheric radionuclide production (Beer et al. 2012). The nature of this mostly stratospheric production (as opposed to tropospheric production), results in a longer mean residence time - ensuring a homogeneous distribution of the cosmogenic radionuclide signature (Beer et al. 2012). The NGRIP ^{10}Be measurements from this study indicate an integrated peak factor increase of 2.40 ± 0.11 relative to background. The ^{10}Be production excess caused by the LU2610 event is therefore a multiple of 100 of SPE05 (X_{05} = 100). By applying this multiple to the spectrum of SPE05, the resulting F_{30} value is 2.0×10^{10} protons.cm^{-2}. This technique has been utilised previously for the AD775 event for ^{10}Be (Mekhaldi et al. 2015), and similarly for ^{14}C (Usoskin et al. 2013).

Additionally, the computed ^{36}Cl production rate for SPE05 was scaled according GRIP ^{36}Cl measurements for the LU2610 event. Computations by Webber et al. (2007) infer that SPE05 resulted in an annual ^{36}Cl production increase of about 5%. The calculated peak factor enhancement (relative to background) for LU2610 ^{36}Cl was 4.57 ± 0.21, resulting in a scaling factor of X_{05}=91. Applying this multiple to SPE05 produces an F30 value of 1.83×10^{10} protons.cm^{-2}. Although we can make the assumption that the transport and deposition mechanisms which control the ^{36}Cl flux are similar to that of ^{10}Be (Beer et al. 2012), the low resolution measurements of ^{36}Cl mean

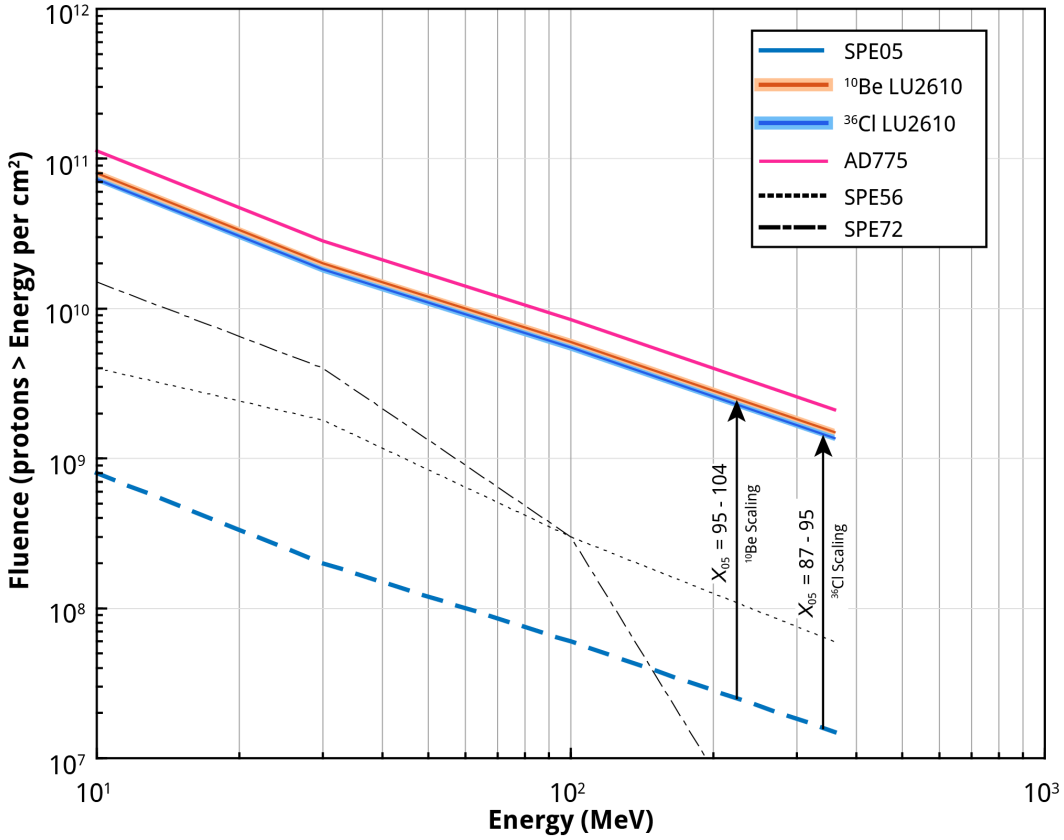

Fig. 16. Estimated fluence spectra of the extreme SPE associated with the LU2610 event based on ^{36}Cl and ^{10}Be and scaled against the fluence spectrum of SPE05 (dashed blue line). Scaling factors for both radionuclides are shown, with shading representing upper and lower uncertainty boundaries. The estimated fluence spectra for AD775 is shown for reference (red line). Dashed black lines indicate spectra for hard (SPE56) and soft (SPE72) events.

F_{30} estimations derived are much less reliable compared to ^{10}Be. The fact that the ^{36}Cl derived F_{30} estimates are within the same magnitude as those calculated from ^{10}Be may suggest some validation in the choice of spectral fit to an instrumentally recorded hard SPE counterpart.

Ultimately, the F_{30} estimates derived from the scaling of LU2610 radionuclide enhancements (and their associated errors) against SPE05 are viewed as upper and lower uncertainty limits, with the actual F_{30} occurring in-between. The estimated LU2610 F_{30} is therefore $1.92 \pm 0.18 \times 10^{10}$ protons.cm^{-2}

5.3 Implications

Based on techniques described in the previous section, the estimated event-integrated fluence spectra of LU2610 are shown in figure 16. These possible fluence spectra estimations involve a series of assumptions and uncertainties in terms of true annually resolved ^{36}Cl peaks, valid ^{10}Be production rates, noise inherent to radionuclide data and the choice of spectral fit. Additionally, we are currently relying on radionuclide records from a single hemisphere to estimate the parameters of a global event.

Nonetheless, several statements can be made with a reasonable level of confidence:

The solar proton event related to the LU2610 radionuclide enhancement is probably stronger than any historical solar flare, including the Carrington event, keeping in mind that the parameters of the Carrington event are still uncertain (Smart et al. 2006).

The event-integrated fluence spectra suggest a fluence > 30 MeV of $1.92 \pm 0.18 \times 10^{10}$ protons.cm^{-2}, indicating that the LU2610 event contained at least an order of magnitude more protons than the so far assumed strongest hard SPE of February 1956 (fig. 15).

Additionally, the LU2610 event was similar in magnitude to the remarkably strong hard AD775 paleo -SPE event (fig. 16). Both the LU2610 and AD775 events resulted in ^{10}Be deposition (inferred here as production) enhancement in polar ice. Furthermore, both events were characterized by a similar hard spectrum and F30 value.

This suggests that solar proton events need to have a hard spectrum and F_{30} values in the region of 10^{10} protons.cm^{-2} in order to leave an imprint on polar ice ^{10}Be concentrations, implying that ^{10}Be is limited to detecting paleo-SPEs with hard spectrum and large F_{30} values.

Alternatively, ^{36}Cl appears to be a better detection method for a wider energy and spectral range of past solar proton events, due to a resonance near ~25-30 MeV for production from ^{40}Ar (Webber et al. 2007).

6 Conclusions

- Of the two supposed sharp increases in IntCal13 which prompted this study, only LU2610 had a synchronous peak in ^{10}Be (NGRIP) and ^{36}Cl (GRIP).
- New sub-annually to annually-resolved ^{10}Be measurements from the NGRIP ice core have led to the discovery of a sharp peak in ^{10}Be deposition around 2610 BP, with an estimated integral increase of 240% relative to annual background ^{10}Be deposition.
- Existing measurements indicate a synchronous ^{36}Cl deposition peak in the GRIP ice core, with an estimated increase of 457% relative to annual background ^{36}Cl deposition.
- The enhancement in ^{36}Cl and ^{10}Be (GRIP and NGRIP), combined with the rapid change in Δ^{14}C in IntCal13, are interpreted here as peak in radionuclide production which is unrelated to normal solar modulation of galactic cosmic rays.
- The peak in production is unlikely to be the result of a supernova explosion, due to the lack of an appropriate remnant signature (relatively recent and relatively close to Earth).
- The arctic ^{10}Be production peak is inconsistent with a short gamma-ray burst per the production mechanisms proposed by Pavlov et al (2013).
- The production enhancement in ^{10}Be and ^{36}Cl matches the expected production increase due to solar protons, and, based on currently available data, a solar proton event is hypothesised as the cause for the LU2610 peak.
- Based on relative ^{36}Cl/^{10}Be ratios, it is suggested that the solar proton event related to LU2610 had a very hard energy spectrum, similar to that of the instrumentally recorded SPE in January 2005.
- The fluence (>30MeV) for the SPE of LU2610 is estimated to be $1.92 \pm 0.18 \times 10^{10}$ protons.cm^{-2}.
- The estimated fluence suggests that the SPE related to LU2610 was much stronger than the Carrington event of 1859 - previously considered as the strongest historically recorded solar flare. It is noted that the strength of the Carrington event has been estimated based on nitrate records (a controversial technique; Wolff et al. (2008)), and corresponding radionuclide spikes relating to this event have not been found.
- The SPE related to LU2610 was at least an order of magnitude more energetic than the so far assumed strongest hard SPE of February 1956, and similar in magnitude to the remarkably strong and hard AD775 paleo-SPE event.

- Due to a resonance near ~25-30 MeV for production from argon-40, chlorine-36 atmospheric production is more sensitive to solar protons than ^{10}Be and ^{14}C. Hence it is suggested as the best detection method of past solar proton events.

- The availability of corresponding annually resolved ^{14}C measurements for the LU2610 period may provide further support for the hypothesis of an SPE source for the LU2610 ^{10}Be/^{36}Cl radionuclide enhancement.

7 Acknowledgements

Firstly, I would like to thank my supervisors Raimund Muscheler and Florian Mekhaldi for giving me the opportunity to work on such an interesting project, for helping me to review my manuscript and for their valuable time taken helping me to discuss ideas and resolve challenges. Additionally, I would like to thank Emma Nilsson for her expert instruction on the preparation of samples for AMS measurement, as well as the staff at the Tandem Laboratory, University of Uppsala, Sweden for the AMS measurements. I would also like to thank Anders Svenson and Lars Berg Larsen from the Center for Ice and Climate in Copenhagen, Denmark for allowing us to sample the NGRIP ice core. Finally, I would like to thank my family and most especially my lovely partner Hannah, for always being such an amazing source of support from half a world away.

8 References

Ackermann, M., Ajello, M., Allafort, A., Baldini, L., Ballet, J., Barbiellini, G., Baring, M., Bastieri, D., Bechtol, K. & Bellazzini, R., 2013: Detection of the characteristic pion-decay signature in supernova remnants. *Science 339*, 807-811.

Adolphi , F. & Muscheler, R., 2016: Synchronizing the Greenland ice core and radiocarbon timescales over the Holocene–Bayesian wiggle-matching of cosmogenic radionuclide records. *Climate of the Past 12*, 15-30.

Andersen, K. K., Svensson, A., Johnsen, S. J., Rasmussen, S. O., Bigler, M., Röthlisberger, R., Ruth, U., Siggaard-Andersen, M.-L., Steffensen, J. P. & Dahl-Jensen, D., 2006: The Greenland ice core chronology 2005, 15–42ka. Part 1: Constructing the time scale. *Quaternary Science Reviews 25*, 3246-3257.

Arnaud, L., Barnola, J. M. & Duval, P., 2000: Physical modeling of the densification of snow/firn and ice in. *Ann. Glaciol 26*, 39-44.

Beer, J., 2000: Long-term indirect indices of solar variability. *Space Science Reviews 94*, 53-66.

Beer, J., Mccracken, K. & Von Steiger, R., 2012: *Cosmogenic Radionuclides: Theory and Applications in the Terrestrial and Space Environments*. Springer Science & Business Media.

Berggren, A. M., Beer, J., Possnert, G., Aldahan, A., Kubik, P., Christl, M., Johnsen, S. J., Abreu, J. & Vinther, B., 2009: A 600-year annual 10Be record from the NGRIP ice core, Greenland. *Geophysical Research Letters 36*.

Bleichrodt, J., 1978: Mean tropospheric residence time of cosmic-ray-produced beryllium 7 at north temperate latitudes. *Journal of Geophysical Research: Oceans 83*, 3058-3062.

Brakenridge, G. R., 2011: Core-collapse supernovae and the Younger Dryas/terminal Rancholabrean extinctions. *Icarus 215*, 101-106.

Burrows, A., 2000: Supernova explosions in the universe. *Nature 403*, 727-733.

Cane, H., Mcguire, R. & Von Rosenvinge, T., 1986: Two classes of solar energetic particle events associated with impulsive and long-duration soft X-ray flares. *The Astrophysical Journal 301*, 448-459.

Castagnoli, G. & Lal, D., 1980: Solar modulation effects in terrestrial production of carbon-14. *Radiocarbon 22*, 133-158.

Chmeleff, J., Von Blanckenburg, F., Kossert, K. & Jakob, D., 2010: Determination of the 10 Be half-life by multicollector ICP-MS and liquid scintillation counting. *Nuclear Instruments and Methods in Physics Research Section B: Beam Interactions with Materials and Atoms 268*, 192-199.

Damon, P. E., Kaimei, D., Kocharov, G. E., Mikheeva, I. B. & Peristykh, A. N., 1995: Radiocarbon production by the gamma-ray component of supernova explosions. *Radiocarbon 37*, 599-604.

Delmas, R., Beer, J., Synal, H. A., Muscheler, R., Petit, J. R. & Pourchet, M., 2004: Bomb-test 36Cl measurements in Vostok snow (Antarctica) and the use of 36Cl as a dating tool for deep ice cores. *Tellus B 56*, 492-498.

Gopalswamy, N., Lara, A., Yashiro, S., Nunes, S. & Howard, R. A., 2003: Coronal mass ejection activity during solar cycle 23. *Solar Variability as an Input to the Earth's Environment.* 403-414 pp.

Gordon, M., Goldhagen, P., Rodbell, K., Zabel, T., Tang, H., Clem, J. & Bailey, P., 2004: Measurement of the flux and energy spectrum of cosmic-ray induced neutrons on the ground. *IEEE Transactions on Nuclear Science 51*, 3427-3434.

Gundestrup, N., 2000: NGRIP field season report 2000.

Hambaryan, V. & Neuhäuser, R., 2013: A Galactic short gamma-ray burst as cause for the 14C peak in AD 774/5. *Monthly Notices of the Royal Astronomical Society*, sts378.

Heikkilä, U., Beer, J. & Feichter, J., 2009: Meridional transport and deposition of atmospheric 10 Be. *Atmospheric Chemistry and Physics 9*, 515-527.

Heikkilä , U. & Smith, A., 2013: Production rate and climate influences on the variability of 10Be deposition simulated by ECHAM5-HAM: Globally, in Greenland, and in Antarctica. *Journal of Geophysical Research: Atmospheres 118*, 2506-2520.

Herbst, K., 2013: *Interaction of cosmic rays with the Earth's magnetosphere and atmosphere*. Ph. D. thesis, University of Kiel, Germany.

Herbst, K., Kopp, A. & Heber, B., 2013: Influence of the terrestrial magnetic field geometry on the cutoff rigidity of cosmic ray particles. *Annales Geophysicae.* Copernicus GmbH. 1637 pp.

Huggle, D., Blinov, A., Stan-Sion, C., Korschinek, G., Scheffel, C., Massonet, S., Zerle, L., Beer, J., Parrat, Y. & Gaeggeler, H., 1996: Production of cosmogenic 36 Cl on atmospheric argon. *Planetary and Space Science 44*, 147-151.

Jackman, C. H., Deland, M. T., Labow, G. J., Fleming, E. L., Weisenstein, D. K., Ko, M. K., Sinnhuber, M., Anderson, J. & Russell, J. M., 2005: The influence of the several very large solar proton events in years 2000–2003 on the neutral middle atmosphere. *Advances in Space Research 35*, 445-450.

Kouveliotou, C., Meegan, C. A., Fishman, G. J., Bhat, N. P., Briggs, M. S., Koshut, T. M., Paciesas, W. S. & Pendleton, G. N., 1993: Identification of two classes of gamma-ray bursts. *The Astrophysical Journal 413*, L101-L104.

Kovaltsov, G., Usoskin, I., Cliver, E., Dietrich, W. & Tylka, A., 2014: Fluence ordering of solar energetic proton events using cosmogenic radionuclide data. *Solar Physics 289*, 4691-4700.

Kovaltsov, G. A., Mishev, A. & Usoskin, I. G., 2012: A new model of cosmogenic production of radiocarbon 14 C in the atmosphere. *Earth and Planetary Science Letters 337*, 114-120.

Koyama, K., Gotthelfii, V. & I-Lwangi, U., 1995: Evidence for shock acceleration of high-energy electrons in the. *Nature 378*, 16.

Lal, D. & Peters, B. 1967: Cosmic ray produced radioactivity on the earth. *In Kosmische Strahlung II/Cosmic Rays II*, 551-612. Springer,

Lee, J.-Y., Marti, K., Severinghaus, J. P., Kawamura, K., Yoo, H.-S., Lee, J. B. & Kim, J. S., 2006: A redetermination of the isotopic abundances of atmospheric Ar. *Geochimica et Cosmochimica Acta 70*, 4507-4512.

Masarik, J. & Beer, J., 1999: Simulation of particle fluxes and cosmogenic nuclide production in the Earth's atmosphere. *Journal of Geophysical Research: Atmospheres 104*, 12099-12111.

Mccracken, K., 2001: Variations in the production of 10Be due to the 11 year modulation of the cosmic radiation, and variations in the vector geomagnetic dipole. *Proceedings of ICRC.*

Mchargue, L. & Damon, P., 1991: The global beryllium 10 cycle. *Reviews of Geophysics 29*, 141-158.

Mekhaldi, F., 2014: The cosmic-ray events around AD 775 and AD 993: assessing their causes and possible effects on climate. *Dissertations in Geology at Lund University*.

Mekhaldi, F., Muscheler, R., Adolphi, F., Aldahan, A., Beer, J., Mcconnell, J. R., Possnert, G., Sigl, M., Svensson, A. & Synal, H.-A., 2015: Multiradionuclide evidence for the solar origin of the cosmic-ray events of AD 774/5 and 993/4. *Nature communications 6*.

Melott, A. L. & Thomas, B. C., 2011: Astrophysical ionizing radiation and Earth: a brief review and census of intermittent intense sources. *Astrobiology 11*, 343-361.

Melott, A. L. & Thomas, B. C., 2012: Causes of an AD 774-775 14C increase. *Nature 491*, E1-E2.

Meyer, P., Parker, E. & Simpson, J., 1956: Solar cosmic rays of February, 1956 and their propagation through interplanetary space. *Physical Review 104*, 768.

Miyake, F., Nagaya, K., Masuda, K. & Nakamura, T., 2012: A signature of cosmic-ray increase in AD 774-775 from tree rings in Japan. *Nature 486*, 240-242.

Muscheler, R., Adolphi, F., Herbst, K. & Nilsson, A., 2016: The revised sunspot record in comparison to cosmogenic radionuclide-based solar activity reconstructions. *Solar Physics 291*, 3025-3043.

Muscheler, R. A., 2000: Nachweis von Änderungen im Kohlenstoffkreislauf durch Vergleich der Radionuklide 10Be, 36Cl und 14C (Doctoral dissertation).

Muscheler, R., Beer, J. & Vonmoos, M., 2004: Causes and timing of the 8200yr BP event inferred from the comparison of the GRIP 10 Be and the tree ring Δ 14 C record. *Quaternary Science Reviews 23*, 2101-2111.

Nakar, E., 2007: Short-hard gamma-ray bursts. *Physics Reports 442*, 166-236.

Pavlov, A., Blinov, A., Konstantinov, A., Ostryakov, V., Vasilyev, G., Vdovina, M. & Volkov, P., 2013: AD 775 pulse of cosmogenic radionuclides production as imprint of a Galactic gamma-ray burst. *Monthly Notices of the Royal Astronomical Society*, stt1468.

Raisbeck, G., Yiou, F., Fruneau, M., Loiseaux, J., Lieuvin, M. & Ravel, J., 1981: Cosmogenic 10Be/7Be as a probe of atmospheric transport processes. *Geophysical Research Letters 8*, 1015-1018.

Reasoner, D. L., Eather, R. & O'brien, B., 1968: Detection of alpha particles in auroral phenomena. *Journal of Geophysical Research 73*, 4185-4198.

Reimer, P. J., Bard, E., Bayliss, A., Beck, J. W., Blackwell, P. G., Bronk Ramsey, C., Buck, C. E., Cheng, H., Edwards, R. L. & Friedrich, M., 2013: IntCal13 and Marine13 radiocarbon age calibration curves 0-50,000 years cal BP.

Schrijver, C., Beer, J., Baltensperger, U., Cliver, E., Güdel, M., Hudson, H., Mccracken, K., Osten, R., Peter, T. & Soderblom, D., 2012: Estimating the frequency of extremely energetic solar events, based on solar, stellar, lunar, and terrestrial records. *Journal of Geophysical Research: Space Physics 117*.

Shea, M. & Smart, D., 1970: On the application of trajectory-derived cutoff rigidities to cosmic-ray intensity variations. *International Cosmic Ray Conference.* 533 pp.

Shea, M. & Smart, D., 1990: A summary of major solar proton events. *Solar Physics 127*, 297-320.

Shea, M. & Smart, D., 2006: Compendium of the eight articles on the "Carrington Event" attributed to or written by Elias Loomis in the American Journal of Science, 1859–1861. *Advances in Space Research 38*, 313-385.

Siegenthaler, U., 1983: Uptake of excess CO2 by an outcrop-diffusion model of the ocean. *Journal of Geophysical Research: Oceans 88*, 3599-3608.

Smart, D., Shea, M. & Mccracken, K., 2006: The Carrington event: Possible solar proton intensity–time profile. *Advances in Space Research 38*, 215-225.

Stauffer, B., 1991: The Greenland Icecore Project (GRIP). Communications. *The Journal of the European Science Foundation 24*, 12-13.

Synal, H.-A., Beer, J., Bonani, G., Suter, M. & Wölfli, W., 1990: Atmospheric transport of bomb-produced 36 Cl. *Nuclear Instruments and Methods in Physics Research Section B: Beam Interactions with Materials and Atoms 52*, 483-488.

Tosaki, Y., Tase, N., Sasa, K., Takahashi, T. & Nagashima, Y., 2012: Measurement of the 36 Cl deposition flux in central Japan: natural background levels and seasonal variability. *Journal of environmental radioactivity 106*, 73-80.

Turekian, K. Y., Nozaki, Y. & Benninger, L. K., 1977: Geochemistry of atmospheric radon and radon products. *Annual Review of Earth and Planetary Sciences 5*, 227.

Usoskin, I., Kromer, B., Ludlow, F., Beer, J., Friedrich, M., Kovaltsov, G., Solanki, S. & Wacker, L., 2013: The AD775 cosmic event revisited: the Sun is to blame. *Astronomy & Astrophysics 552*, L3.

Usoskin, I. G. & Kovaltsov, G. A., 2008: Production of cosmogenic 7Be isotope in the atmosphere: Full 3-D modeling. *Journal of Geophysical Research: Atmospheres 113*.

Usoskin, I. G. & Kovaltsov, G. A., 2012: Occurrence of extreme solar particle events: assessment from historical proxy data. *The Astrophysical Journal 757*, 92.

Vasiliev, S. & Dergachev, V., 2002: The~ 2400-year cycle in atmospheric radiocarbon concentration: bispectrum of 14 C data over the last 8000 years. Annales Geophysicae. 115-120 pp.

Stuiver, M., & Becker, B.,1993: High-precision decadal calibration of the radiocarbon time scale, AD 1950-6000 BC. *35*, 35-65.

Vinther, B. M., Clausen, H. B., Johnsen, S. J., Rasmussen, S. O., Andersen, K. K., Buchardt, S. L., Dahl-Jensen, D., Seierstad, I. K., Siggaard-Andersen, M. L. & Steffensen, J. P., 2006: A synchronized dating of three Greenland ice cores throughout the Holocene. *Journal of Geophysical Research: Atmospheres 111*.

Vonmoos, M., Beer, J. & Muscheler, R., 2006: Large variations in Holocene solar activity: Constraints from 10Be in the Greenland Ice Core Project ice core. *Journal of Geophysical Research: Space Physics 111*.

Wagner, G., Masarik, J., Beer, J., Baumgartner, S., Imboden, D., Kubik, P. W., Suter, M. 2000: Reconstruction of the geomagnetic field between 20 and 60 kyr BP from cosmogenic radionuclides in the GRIP ice core. *Nuclear Instruments and Methods in Physics Research Section B: Beam Interactions with Materials and Atoms, 172(1), 597-604.*

Webb, D. F. & Howard, R. A., 1994: The solar cycle variation of coronal mass ejections and the solar wind mass flux. *Journal of Geophysical Research: Space Physics 99*, 4201-4220. doi: 10.1029/93JA02742

Webber, W., Higbie, P. & Mccracken, K., 2007: Production of the cosmogenic isotopes 3H, 7Be, 10Be, and 36Cl in the Earth's atmosphere by solar and galactic cosmic rays. *Journal of Geophysical Research: Space Physics 112*.

Wolff, E., Bigler, M., Curran, M., Dibb, J. E., Frey, M., Legrand, M. & Mcconnell, J., 2012: The Carrington event not observed in most ice core nitrate records. *Geophysical Research Letters 39*.

Wolff, E., Jones, A. E., Bauguitte, S.-B. & Salmon, R. A., 2008: The interpretation of spikes and trends in concentration of nitrate in polar ice cores, based on evidence from snow and atmospheric measurements. *Atmospheric Chemistry and Physics 8*, 5627-5634.

Yim, M.-S. & Caron, F., 2006: Life cycle and management of carbon-14 from nuclear power generation. *Progress in Nuclear Energy 48*, 2-36.

Zhou, D., Wang, C., Peng, Z., Rutledge, R., Sun, Y., Liang, J., Zhu, G., Zhang, S., Zhang, B. & Zhou, P., The Solar Cosmic-Ray Origin for the Rapid 14 C Increase in AD775.

Tidigare skrifter i serien ”Examensarbeten i Geologi vid Lunds universitet”:

448. Halling, Jenny, 2015: Inventering av sprickmineraliseringar i en del av Sorgenfrei-Tornquistzonen, Dalby stenbrott, Skåne. (15 hp)
449. Nordas, Johan, 2015: A palynological study across the Ordovician Kinnekulle. (15 hp)
450. Åhlén, Alexandra, 2015: Carbonatites at the Alnö complex, Sweden and along the East African Rift: a literature review. (15 hp)
451. Andersson, Klara, 2015: Undersökning av slugtestsmetodik. (15 hp)
452. Ivarsson, Filip, 2015: Hur bildades Bushveldkomplexet? (15 hp)
453. Glommé, Alexandra, 2015: $^{87}Sr/^{86}Sr$ in plagioclase, evidence for a crustal origin of the Hakefjorden Complex, SW Sweden. (45 hp)
454. Kullberg, Sara, 2015: Using Fe-Ti oxides and trace element analysis to determine crystallization sequence of an anorthosite-norite intrusion, Älgön SW Sweden. (45 hp)
455. Gustafsson, Jon, 2015: När började plattektoniken? Bevis för plattektoniska processer i geologisk tid. (15 hp)
456. Bergqvist, Martina, 2015: Kan Ölands grundvatten öka vid en uppdämning av de utgrävda dikena genom strandvallarna på Ölands östkust? (15 hp)
457. Larsson, Emilie, 2015: U-Pb baddeleyite dating of intrusions in the south-easternmost Kaapvaal Craton (South Africa): revealing multiple events of dyke emplacement. (45 hp)
458. Zaman, Patrik, 2015: LiDAR mapping of presumed rock-cored drumlins in the Lake Åsnen area, Småland, South Sweden. (15 hp)
459. Aguilera Pradenas, Ariam, 2015: The formation mechanisms of Polycrystalline diamonds: diamondites and carbonados. (15 hp)
460. Viehweger, Bernhard, 2015: Sources and effects of short-term environmental changes in Gullmar Fjord, Sweden, inferred from the composition of sedimentary organic matter. (45 hp)
461. Bokhari Friberg, Yasmin, 2015: The paleoceanography of Kattegat during the last deglaciation from benthic foraminiferal stable isotopes. (45 hp)
462. Lundberg, Frans, 2016: Cambrian stratigraphy and depositional dynamics based on the Tomten-1 drill core, Falbygden, Västergötland, Sweden. (45 hp)
463. Flindt, Anne-Cécile, 2016: A pre-LGM sandur deposit at Fiskarheden, NW Dalarna - sedimentology and glaciotectonic deformation. (45 hp)
464. Karlatou-Charalampopoulou, Artemis, 2016: Vegetation responses to Late Glacial climate shifts as reflected in a high resolution pollen record from Blekinge, south-eastern Sweden, compared with responses of other climate proxies. (45 hp)
465. Hajny, Casandra, 2016: Sedimentological study of the Jurassic and Cretaceous sequence in the Revinge-1 core, Scania. (45 hp)
466. Linders, Wictor, 2016: U-Pb geochronology and geochemistry of host rocks to the Bastnäs-type REE mineralization in the Riddarhyttan area, west central Berglsagen, Sweden. (45 hp)
467. Olsson, Andreas, 2016: Metamorphic record of monazite in aluminous migmatitic gneisses at Stensjöstrand, Sveconorwegian orogen. (45 hp)
468. Liesirova, Tina, 2016: Oxygen and its impact on nitrification rates in aquatic sediments. (15 hp)
469. Perneby Molin, Susanna, 2016: Embryologi och tidig ontogeni hos mesozoiska fisködlor (Ichthyopterygia). (15 hp)
470. Benavides Höglund, Nikolas, 2016: Digitization and interpretation of vintage 2D seismic reflection data from Hanö Bay, Sweden. (15 hp)
471. Malmgren, Johan, 2016: De mellankambriska oelandicuslagren på Öland - stratigrafi och faciestyper. (15 hp)
472. Fouskopoulos Larsson, Anna, 2016: XRF -studie av sedimentära borrkärnor - en metodikstudie av programvarorna Q-spec och Tray-sum. (15 hp)
473. Jansson, Robin, 2016: Är ERT och Tidsdomän IP potentiella karteringsverktyg inom miljögeologi? (15 hp)
474. Heger, Katja, 2016: Makrofossilanalys av sediment från det tidig-holocena undervattenslandskapet vid Haväng, östra Skåne. (15 hp)
475. Swierz, Pia, 2016: Utvärdering av vattenkemisk data från Borgholm kommun och dess relation till geologiska förhållanden och markanvändning. (15

hp)

476. Mårdh, Joakim, 2016: WalkTEM-undersökning vid Revingehed provpumpningsanläggning. (15 hp)
477. Rydberg, Elaine, 2016: Gummigranulat - En litteraturstudie över miljö- och hälsopåverkan vid användandet av gummigranulat. (15 hp)
478. Björnfors, Mark, 2016: Kusterosion och äldre kustdyners morfologi i Skälderviken. (15 hp)
479. Ringholm, Martin, 2016: Klimatutlöst matbrist i tidiga medeltida Europa, en jämförande studie mellan historiska dokument och paleoklimatarkiv. (15 hp)
480. Teilmann, Kim, 2016: Paleomagnetic dating of a mysterious lake record from the Kerguelen archipelago by matching to paleomagnetic field models. (15 hp)
481. Schönström, Jonas, 2016: Resistivitets- och markradarmätning i Ängelholmsområdet - undersökning av korrosiva markstrukturer kring vattenledningar. (15 hp)
482. Martell, Josefin, 2016: A study of shock-metamorphic features in zircon from the Siljan impact structure, Sweden. (15 hp)
483. Rosvall, Markus, 2016: Spår av himlakroppskollisioner - bergarter i nedslagskratrar med fokus på Mien, Småland. (15 hp)
484. Olausson, My, 2016: Resistivitets- och IP -mätningar på den nedlagda deponin Gustavsfält i Halmstad. (30 hp)
485. Plan, Anders, 2016: Markradar- och resistivitetsmätningar – undersökningar utav korrosionsförhöjande markegenskaper kring fjärrvärmeledningar i Ängelholm. (15 hp)
486. Jennerheim, Jessica, 2016: Evaluation of methods to characterise the geochemistry of limestone and its fracturing in connection to heating. (45 hp)
487. Olsson, Pontus, 2016: Ekologiskt vatten från Lilla Klåveröd: en riskinventering för skydd av grundvatten. (15 hp)
488. Henriksson, Oskar, 2016: The Dynamics of Beryllium 10 transport and deposition in lake sediments. (15 hp)
489. Brådenmark, Niklas, 2016: Lower to Middle Ordovician carbonate sedimentology and stratigraphy of the Pakri peninsula, north-western Estonia. (45 hp)
490. Karlsson, Michelle, 2016: Utvärdering av metoderna DCIP och CSIA för identifiering av nedbrytningszoner för klorerade lösningsmedel: En studie av Färgaren 3 i Kristianstad. (45 hp)
491. Elali, Mohammed, 2016: Flygsanddyners inre uppbyggnad – georadarundersökning. (15 hp)
492. Preis-Bergdahl, Daniel, 2016: Evaluation of DC Resistivity and Time-Domain IP Tomography for Bedrock Characterisation at Önneslöv, Southern Sweden. (45 hp)
493. Kristensson, Johan, 2016: Formation evaluation of the Jurassic Stø and Nordmela formations in exploration well 7220/8-1, Barents Sea, Norway. (45 hp)
494. Larsson, Måns, 2016: TEM investigation on Challapampa aquifer, Oruro Bolivia. (45 hp)
495. Nylén, Fredrik, 2017: Utvärdering av borrhålskartering avseende kalksten för industriella ändamål, File Hajdarbrottet, Slite, Gotland. (45 hp)
496. Mårdh, Joakim, 2017: A geophysical survey (TEM; ERT) of the Punata alluvial fan, Bolivia. (45 hp)
497. Skoglund, Wiktor, 2017: Provenansstudie av detriala zirkoner från ett guldförande alluvium vid Ravlunda skjutfält, Skåne. (15 hp)
498. Bergcrantz, Jacob, 2017: Ett fönster till Kattegatts förflutna genom analys av bottenlevande foraminiferer. (15 hp)
499. O'Hare, Paschal, 2017: Multiradionuclide evidence for an extreme solar proton event around 2610 BP. (45 hp)

LUNDS UNIVERSITET

Geologiska institutionen
Lunds universitet
Sölvegatan 12, 223 62 Lund